Allosteric effector ppGpp potentiates the inhibition of transcript initiation by DksA

Vadim Molordtsov[1], Elena Sineva[1], Lu Zhang[2], Xuhui Huang[3], Michael Cashel[4], Sarah E. Ades[1,5], Katsuhiko S. Murakami[1,5,6]

[1]Department of Biochemistry and Molecular Biology, The Center for RNA Molecular Biology, The Pennsylvania State University, University Park, PA 16802, USA

[2]State Key Laboratory of Structural Chemistry, Fujian Institute of Research on the Structure of Matter, Chinese Academy of Sciences, Fuzhou, Fujian, 350002, China

[3]Department of Chemistry, The Hong Kong University of Science and Technology, Clear Water Bay, Kowloon, Hong Kong

[4]Intramural Research Program, Eunice Kennedy Shriver, National Institute of Child Health and Human Development, National Institutes of Health, Bethesda, MD 20892, USA

[5]Correspondence: kum14@psu.edu, ades@psu.edu

[6]Lead contact: kum14@psu.edu

Highlights

- DksA has two modes of binding to RNA polymerase
- DksA is capable of inhibiting the catalysis and influences the DNA binding of RNAP
- ppGpp acts as an allosteric effector of DksA function
- ppGpp stabilizes DksA in a more functionally important binding mode

SUMMARY

DksA and ppGpp are the central players in the *Escherichia coli* stringent response and mediate a complete reprogramming of the transcriptome from one optimized for rapid growth to one adapted for survival during nutrient limitation. A major component of the response is a reduction in ribosome synthesis, which is accomplished by the synergistic action of DksA and ppGpp bound to RNA polymerase (RNAP) inhibiting transcription of rRNAs. Here, we report the X-ray crystal structures of *E. coli* RNAP holoenzyme in complex with DksA alone and with ppGpp. The structures show that DksA accesses the catalytic and the DNA binding sites of RNAP simultaneously, and reveal that binding of the allosteric effector ppGpp reshapes the RNAP–DksA complex and potentiates the inhibition of rRNA promoters by DksA. We also determined the structure of RNAP–TraR complex, which reveals the mechanism of ppGpp-independent transcription inhibition by TraR. This work establishes new ground for understanding the pleiotropic effects of DksA and ppGpp on transcriptional regulation in proteobacteria.

INTRODUCTION

The stringent response in bacteria is a global rearrangement of cellular metabolism from one optimized for vegetative growth to one optimized for stress survival and is accompanied by an alternation in the expression of over 500 genes (Durfee et al., 2008) including those involved in ribosome biogenesis, amino acid synthesis, virulence, survival during host invasion, antibiotic resistance and persistence (Dalebroux and Swanson, 2012; Hauryliuk et al., 2015; Potrykus and Cashel, 2008). Accumulation of unusual nucleotides, the bacterial alarmones ppGpp (guanosine tetraphosphate) and pppGpp (guanosine pentaphosphate), collectively abbreviated as ppGpp, triggers the stringent response. In the proteobacteria, ppGpp exerts its effects on gene expression primarily by binding to RNAP.

Transcriptional regulation by ppGpp has been studied most extensively in *E. coli*. Unlike DNA-binding transcriptional regulators, which exert their effects only on genes with regulator binding sites properly positioned relative to the RNAP binding site, ppGpp binds to RNAP and has the potential to influence the expression of any genes. Whether expression of any given gene is altered by ppGpp, is determined by the properties of the promoter directing expression of that

gene (Haugen et al., 2008). Many genes are unaffected by ppGpp while others are repressed, notably those encoding stable rRNAs, or activated, including genes for amino acid biosynthesis.

ppGpp often works in conjunction with DksA, a 17.5 kDa protein conserved in proteobacteria, DksA belongs to the class of RNAP secondary channel binding transcription factors that includes GreA and GreB (Opalka et al., 2003; Sekine et al., 2015), Gfh1 (Tagami et al., 2010) and TraR (Blankschien et al., 2009b) (**SFigs. 1A, B and C**). It has been proposed that DksA potentiates the regulation of rRNA transcription in response to changing concentrations of ppGpp and initiating NTP (iNTP) under different growth conditions (Paul et al., 2004; Perederina et al., 2004). The crystal structure of DksA showed that it consists of five α helixes organized into three structural parts (**SFig. 1A**) (Perederina et al., 2004). The globular domain (G domain) is formed by amino acids from residues 1-32 and 109-134 and includes two α helixes (α_1 and α_4) along with the Zn binding region. The central segment of the polypeptide chain (residues 33-108) forms an extended coiled-coil domain (CC domain) with two long α-helices (α_2 and α_3) connected by a short linker (CC tip). The C-terminal end of DksA forms an extended α helix (CT-helix, residues 135–151), which is loosely connected to the rest of the protein. The structural organization of DksA is similar to that of the Gre factors and Gfh1, which also contain the G and CC domains, however, the CT-helix is present only in DksA.

Phenotypes of a Δ*dksA* strain partially overlap with those of a strain deficient in ppGpp synthesis, particularly during amino acid starvation, the classical stringent response condition suggesting that the act synergistically. The cellular concentration of DksA remains constant under different growth conditions and, consequently, its function as a transcriptional regulator is enhanced by ppGpp (Paul et al., 2004; Paul et al., 2005; Rutherford et al., 2007). Binding of DksA to RNAP reduces the stability of most of RNAP–promoter complexes, however, the outcomes of DksA and ppGpp action, repression, lack of effect or activation, are promoter-specific and likely depend on where the rate-limiting step occurs in the transition from the closed promoter complex (RPc) to the transcription initiation (Paul et al., 2004; Paul et al., 2005; Rutherford et al., 2009). DksA and ppGpp have been shown to decrease the life time of open complexes (RPo) formed by RNAP on all promoters. For those promoters that form short-lived RPo, further reduction in its stability favors accumulation of the RPc and dissociation of RNAP from the promoter, ultimately resulting in inhibition of transcript initiation. Although DksA and ppGpp will reduce the stability of RPo for promoters that form longer-lived RPo, it is not

limiting for transcription initiation and these promoters are not inhibited. As such, it appears that a defining characteristic of promoters subject to negative regulation by ppGpp and DksA is formation of an intrinsically unstable RPo such as ribosomal promoters.

The ppGpp binding site of *E. coli* RNAP was identified at a cavity surrounded by α, β' and ω subunits (Mechold et al., 2013; Ross et al., 2013; Zuo et al., 2013). Although RNAP reconstituted without the ω subunit was no longer inhibited by ppGpp *in vitro* in the absence of DksA (Igarashi et al., 1989), deletion of the *E. coli* gene encoding ω (*rpoZ*) resulted relatively mild phenotypes *in vivo* (Gentry et al., 1991), suggesting that this ppGpp binding site (hereafter referred to as site 1) is insufficient for induction of the stringent response. A recent study identified another ppGpp binding site near the secondary channel of RNAP, which is ~60 Å away from the site 1 (Ross et al., 2016). This second ppGpp binding site (hereafter referred to as site 2) is formed only in the presence of DksA. The growth rate of an *E. coli* strain with a variant of RNAP carrying mutations that disrupt site 2 is severely impaired in minimal medium as would be expected if ppGpp binding at site 2 were primarily responsible for reprogramming gene expression during the stringent response (Ross et al., 2016). A structural analysis of the RNAP and DksA complex with and without ppGpp is required to better elucidate the mechanism of DksA and ppGpp synergism in transcriptional regulation, particularly how ppGpp binding enhances the transcriptional regulatory activity of DksA.

The small, 73 amino acids long transcription regulator, TraR binds in the secondary channel of RNAP similar to DksA (Blankschien et al., 2009b; Grace et al., 2015). Although the full spectrum of TraR functions in cell metabolism remains to be determined, it is often found in conjugative plasmids that enable horizontal gene transfer, and it has been proposed to play a role in bacterial antibiotic resistance, pathogenicity and virulence (Maneewannakul and Ippen-Ihler, 1993). TraR is a truncated version of DksA, lacking the first 68 amino acids, it can inhibit transcription of ribosomal genes and activate transcription of amino acid biosynthesis genes (Gopalkrishnan et al., 2017). Interestingly, TraR function is not influenced by ppGpp, therefore, investigation of the structure and function of TraR may lead to better understanding of the synergism between DksA and ppGpp in transcription regulation.

In this study, we report the crystal structures of the *E. coli* RNAP σ^{70} holoenzyme–DksA complex with and without ppGpp. The structures reveal the precise interaction network among RNAP, DksA and ppGpp, and provide insights into the basis for transcription inhibition by these

factors. Conformational changes are observed in both RNAP and DksA during the binary complex (RNAP–DksA) and the ternary complex (RNAP–DksA/ppGpp) formations that have implications for the mechanism of transcriptional regulation. Importantly, the location of DksA is altered by ppGpp binding providing an explanation for how ppGpp allosterically potentiates the function of DksA. We also determined the crystal structure of RNAP in complex with TraR and established the mechanism by which this small secondary channel binding protein effectively regulates transcription without ppGpp.

RESULTS

The structure of the RNAP–DksA binary complex

Because the secondary channel of RNAP is widely opened in the crystalline state of the *E. coli* RNAP σ^{70} holoenzyme (Murakami, 2013), we chose to prepare co-crystals of the RNAP–DksA complex by soaking DksA into preformed RNAP crystals and determined its X-ray structure (**Table 1**). A similar approach had been used for reconstitution of yeast RNAP II with the transcription factor TFIIS, which also binds at the secondary channel of RNAP II (Kettenberger et al., 2003). It is interesting to note that the crystal lattice can tolerate large structural rearrangements induced by DksA and also ppGpp, which is described later (**The structure of the RNAP–DksA/ppGpp ternary complex**). Since all structures were obtained from the same crystal form and crystal packing, the detected structural changes were attributed to either DksA binding to RNAP or accommodation of ppGpp. The crystal structures of RNAP (Murakami, 2013) and DksA (Perederina et al., 2004) can be fitted to the electron density map without ambiguity (**SFig. 2A**). The electron density map of the CC domain of DksA is well defined in the binary complex; however, the electron density map of the G domain is scattered and discontinuous (**SFig. 1D**), indicating that DksA is not stably bound to RNAP without ppGpp.

DksA primarily contacts the β' subunit and 1,633 $Å^2$ of its surface is involved in the interaction with RNAP (**Fig. 1**). All three parts of DksA including the CC and G domains and the CT-helix are involved in the assembly with RNAP. The CC domain is positioned in a cleft on RNAP that runs from the secondary to the main channels. One surface of the DksA CC domain faces the β'rim helix and runs alongside it but makes few physical interactions. The opposite surface of CC domain faces the β'i6 (also known as β'SI3) (Chlenov et al., 2005), a lineage specific insertion domain located in the middle of trigger loop. Due to its flexible nature, the β'i6

could not be resolved in any of the structures determined in this study. The G domain binds at the edge of β'rim helix causing a 7.2 Å shift in its position compared with the apo-form RNAP (**Fig. 2C, SMovie 1**). The CT-helix extends toward the βlobe/i4 domain (**Figs. 1 and 2A**), which forms one of pincers of the DNA binding channel (**Fig. 2A**) and is also essential for DksA-dependent transcriptional regulation (Parshin et al., 2015). DksA binding to RNAP, likely mediated by the CT-helix, rotates the βlobe/i4 domain as a rigid body toward the β'rim helix (**Fig. 2C, SMovie 1**). The conformation of DksA itself also changes upon RNAP binding; the α_1, α_4 and CT-helix move in different directions from the center of G domain, weakening the hydrophobic packing between the CC and G domains (**Fig. 2F, SMovie 2**).

The tip of the CC domain inserts into the secondary channel and reaches within ~16 Å of the catalytic Mg^{2+} in the active site of RNAP (**Fig. 2A**). Amino acid substitutions at the CC tip (D74 and A76) eliminate DksA function without affecting its apparent affinity for RNAP (Lee et al., 2012); these residues approach the bridge helix but do not directly contact with it. However, a positon of the CC domain of DksA suggests that it prevents folding of the trigger loop (**Fig. 2A, SFig. 3A**), which is essential for the catalytic step of RNA synthesis (Yuzenkova et al., 2010; Zhang et al., 2010), indicating that DksA is capable of repressing transcription by restricting the catalytic activity of RNAP in addition to destabilize the RPo.

The structure of the RNAP–DksA/ppGpp ternary complex

We prepared co-crystals of the ternary complex containing RNAP, DksA and ppGpp in the same manner as the RNAP–DksA complex, by stepwise soaking of DksA and then ppGpp into RNAP crystals (**Table 1**). Extra electron densities corresponding to ppGpp molecules were found at the location previously describe for ppGpp binding site 1 and the interface of the β'rim helix and DksA as predicted for ppGpp binding site 2 from biochemical and genetic studies (**SFigs. 2B and C**). Sites 1 and 2 are separated from each other by 62 Å, and by 31 and 40 Å from the active site, respectively (**Fig. 3A**) indicating that they do not function via direct interactions with each other or the active site.

The chemical environments of the ppGpp binding sites 1 and 2 are distinct. Site 1 appears as a dimple on the interface between β' and ω subunits and is covered by one of α subunits. ppGpp uses one of its molecular surfaces for binding to RNAP while exposing the flipside to solvent (**Fig. 3B**). The guanine base is sandwiched by side chains of R362 and I619 of the β'

subunit in addition to forming a hydrogen bond with H364 and a salt bridge with D622 side chains. In sharp contrast, site 2 is located in a narrow pocket at the interface between DksA and the β'rim helix. The guanine base of ppGpp inserts into the cleft, while the sugar and phosphate groups remain solvent exposed (**Fig. 3C**). DksA mainly participates by forming salt bridges between basic residues from α_3 of the CC domain and the CT-helix (R91, K94, K98 and K139) and the phosphate backbone of ppGpp (**Fig. 3D**). In addition, L95 side chain contacts the guanine base by van der Waals interaction and R129 participates in charge neutralization of E677 of β' subunit, which locates near the 5' diphosphate group of ppGpp. In contrast, the β'rim helix contributes to the guanine base interaction by a salt bridge (D684), a hydrogen bond (N680) and van der Waals contacts (Y679, N680 and I683). Substitutions of several of these residues reduced the effect of DksA and ppGpp on transcript initiation (Parshin et al., 2015; Ross et al., 2016).

The electron density of the DksA G domain was enhanced in the ternary complex compared with that in the binary complex (**SFig. 1E**), suggesting that the ppGpp binding at the site 2 stabilizes the RNAP–DksA interaction. Binding of ppGpp also shifts the orientation of DksA, which undergoes a rigid body rotation centered around ppGpp binding site 2 (**Fig. 2B, SMovie 3**). This rotation leads to deeper insertion of the CC domain into the secondary channel, positioning the D71 side chain at the CC tip only 4.5 Å away from the catalytic Mg^{2+} of RNAP. The A76 residue at the CC tip directly contacts the bridge helix and may restrict its movement as well as severely interfere with folding of the trigger loop in the ternary complex (**Fig. 2B, SFig. 3B**). Interestingly, the conformational changes of RNAP triggered by DksA binding, including the dislocations of the β'rim helix and the βlobe/i4 domain, were restored to their original states seen in the apo-form RNAP upon binding of ppGpp (**Figs. 2D and E**). ppGpp appears to facilitate DksA's interactions with RNAP by relieving mechanical stress in the β'rim helix thereby stabilizing the RNAP–DksA interaction and positions the CC tip of DksA in a location that should severely compromise catalysis by RNAP. As a consequence of the repositioning of DksA upon ppGpp binding, the total contact area between DksA and RNAP increases 1.5 folds.

The binding of ppGpp also triggers a conformational change in DksA itself, restoring the partially disordered regions found in the binary complex to the conformation observed in the unbound state (**Figs. 2G and H, SMovie 2**). These movements include shifting of the α_1, α_4 and

CT-helix toward the center of the G domain, swinging of α_2 and α_3 helices in the opposite direction, and slight bending of the CC domain.

The structure of the RNAP–TraR complex

Although TraR appears to be a structural and functional homologue of DksA, ppGpp does not influence its activities (Blankschien et al., 2009b; Gopalkrishnan et al., 2017; Grace et al., 2015). To extend our understanding of the mechanism of transcriptional regulation through the secondary channel, we prepared crystals of the RNAP–TraR complex by soaking TraR into RNAP crystals and determined the structure at 3.8 Å resolution (**Table 1**). Strong electron density corresponding to TraR was observed from the βlobe/i4 domain extending through the secondary channel to the active site (**SFigs. 1F and 2D**), allowing us to build the TraR model (**SFig. 1B**) and refine the RNAP–TraR complex structure (**Fig. 4A**).

TraR contains three α helices (α_1, α_2 and α_3) that can be assigned to three structural regions analogous to DksA (**SFig. 1B**). The N-terminal α_1 helix (NT-helix) of TraR, which is a counterpart of the DksA CC domain (**Fig. 4B**) and fits into the secondary channel of RNAP. Electron density of the N-terminus of TraR is traceable beginning with the glutamate at position 4, which is located only 2.4 Å away from the active site Mg^{2+} of RNAP and appears to be involved in Mg^{2+} coordination (**Fig. 4C**). As seen with D74 of DksA in the ternary complex, the D6 side chain of TraR forms salt bridges with R678/R1106 (β subunit) and R731 (β' subunit) residues near the active site. Mutation of D6 residue severely impaired the TraR function (Blankschien et al., 2009b; Gopalkrishnan et al., 2017). The G domain of TraR contacts the edge of the β'rim helix and contains four Cys residues to coordinate a Zn atom. The CT-helix extends away from the G domain toward the βlobe/i4 domain. Similar to DksA, TraR is able to simultaneously access two important sites when bound to RNAP including the active site and one of the pincers that forms the DNA binding channel.

The NT-helix of TraR extends from the RNAP active site to the outer rim of the secondary channel, following the same path as the CC domain of DksA when bound in the presence of ppGpp (**Fig. 4B**). However, after residue T16, the NT-helix of TraR follows a trajectory that is different from DksA, resulting in tighter association between the NT-helix and G domain of TraR with the β'rim helix. As a consequence, hydrophobic residues I23 and I27 of TraR occupy the space corresponding to ppGpp binding site 2 (**Fig. 4D**). TraR binding does not

trigger any major conformational change in RNAP. As a result, the RNAP–TraR complex is more similar to the RNAP–DksA/ppGpp complex than the RNAP–DksA complex.

NTP entry route to the RNAP active site in the presence of secondary channel binding transcription factors

The CC domains of DksA and NT-helix of TraR fully occupy the secondary channel of RNAP, which has been proposed to serve as the major access route of NTPs to the active site (**SFigs. 4A, B and C**) (Batada et al., 2004; Zhang et al., 2015). This fact raises the question of how NTPs can access the active site of RNAP in the presence of bound DksA or TraR. We therefore explored the possible NTP loading pathways in the RPo containing the DksA or TraR by identifying empty spaces in these complexes available for NTP loading (**SFig. 4E**). Our modeling on the RPo revealed that NTP can be loaded not only through the secondary channel but also via the main channel because only the single stranded DNA is located in the main channel in RPo (**SFig. 4D**) as opposed to a ~9 bp long DNA/RNA hybrid in the elongation complex. Because the NTP loading path through the secondary channel is completely blocked by DksA or TraR, the main channel should become the sole pathway for NTPs to access the active site during transcript initiation in the presence of these factors (**SFig. 4E**).

Determination of the affinities of DksA and TraR to RNAP holoenzyme and the effect of ppGpp

A comparison of the structures of binary and ternary complexes suggests that the synergism observed between DksA and ppGpp could arise from ppGpp increasing the extent of the interaction surface between DksA and RNAP (**Fig. 2B, SMovie 3**), renaturing the DksA (**Fig. 2G, SMovie 2**), and eliminating the energetically unfavorable conformational changes of RNAP seen with DksA binding alone (**Figs. 2C and D**). These activities should increase the affinity of DksA for RNAP. To test this model, we measured the dissociation constant (K_d) of DksA to different forms of RNAP using fluorescence anisotropy assay (**Fig. 5**). A DksA derivative containing an A35C amino acid substitution was constructed and used to conjugate a fluorescent label to DksA. This site was chosen for labeling because it is surface exposed and located in a region, which is not involved in binding to RNAP. Affinity was measured by adding increasing amounts of RNAP to labeled DksA ($DksA^{fl}$) and measuring changes in anisotropy. DksA binds

with slightly lower affinity to the core RNAP compared to the σ^{70} holoenzyme (K_d=112 and 52 nM for core and holoenzymes, respectively) (**Fig. 5A**). When ppGpp is added to the binding reaction, the affinity of DksA to both holoenzyme and core RNAP increases in a concentration-dependent manner (**Figs. 5C and D**).

The structure of TraR bound to RNAP indicates that it makes more extensive contacts with RNAP (**Figs. 4A and B**) and therefore should bind with higher affinity than DksA. To test this hypothesis, we used a competitive binding assay in which the anisotropy of $DksA^{fl}$ bound to RNAP was measured in the presence of increasing amounts of unlabeled TraR or unlabeled DksA. TraR was able to displace $DksA^{fl}$ at significantly lower concentrations than DksA (**Fig. 5B**). Binding constants estimated from the competition experiment indicate that the affinity of TraR with RNAP is 6 nM, which is 8.6 and 3 times higher than the DksA affinity to RNAP in the absence and presence of 100 μM ppGpp, respectively. We also note that the affinity of unlabeled DksA for RNAP measured using the competition experiment is 52 nM, which is comparable to that measured for $DksA^{fl}$ indicating that the fluorescent label does not interfere with binding affinity.

To measure the binding of DksA to DNA-bound RNAP, DksA was incubated with RNAP and several different promoter DNA fragments including promoters that are positively regulated (P*usp*), insensitive (T7A1), differentially regulated (λ_{PR}) and negatively regulated (*rrnB*P1) by DksA and ppGpp (**SFig. 5**) (Gummesson et al., 2013; Lyzen et al., 2009; Paul et al., 2004; Perederina et al., 2004). Promoter DNA was in 6-fold molar excess compared to RNAP. The apparent affinity of DksA with the RNAP–promoter DNA complex was weaker than that for free holoenzyme for all promoters tested. Notably, ppGpp improved DksA binding in all cases (**Figs. 5E and F**). There is an interesting correlation between the apparent DksA affinity and promoter type, *e.g.*, a DksA activated promoter (P*usp*) demonstrated very weak DksA binding even in the presence of ppGpp. The apparent affinities of DksA for the DksA-activated, ppGpp-inhibited λ_{PR} and insensitive T7A1 promoters were greater than that of P*usp*, but less than that observed for the negatively regulated *rrnB*P1 promoter. In fact, the *rrnB*P1 promoter showed a relatively small reduction in DksA binding compared to free RNAP holoenzyme, particularly in the presence of ppGpp. In these assays, there is likely a mixture of free RNAP as well as DNA-bound RNAP, although we sought to minimize the amount of free RNAP by including excess DNA. Therefore, it is likely that the values obtained are somewhat overestimating the actual

binding affinity. We do note that the affinities observed here for P*usp* and λ_{PR} are in the same range as that measured previously using an iron-mediated cleavage assay to detect DksA binding with the consensus "full con" promoter that forms very stable RPo (Lennon et al., 2009).

DISCUSSION

In this study, we present the X-ray crystal structures of the *E. coli* RNAP holoenzyme in complex with DksA in the presence and absence of ppGpp (**Figs. 1 and 2**), which reveals that DksA contacts two important regions of RNAP, active site and DNA binding channel. The structures suggest that DksA is capable of inhibiting the catalysis of RNA synthesis by preventing the folding of trigger loop and also the binding NTP at the active site via the CC domain insertion through the RNAP secondary channel. It also appears that DksA influences the RPo formation of RNAP by restricting the opening and closing of the main channel of RNAP via the CT-helix contacting with the βlobe/i4 domain.

Since ppGpp was discovered nearly 50 years ago as a key regulator of rRNA transcriptions (Cashel and Gallant, 1969), elucidation of the mechanism of regulation initially proved challenging because effects of ppGpp observed *in vitro* could not fully account for the magnitude of the effects seen *in vivo*. The discovery of DksA and finding that it potentiated the effects of ppGpp significantly advanced our understanding of the regulation (Paul et al., 2004; Perederina et al., 2004). It has been proposed that DksA enhances the regulatory function of ppGpp as its cofactor (Haugen et al., 2008; Hauryliuk et al., 2015; Potrykus and Cashel, 2008). In this study, we revealed that distortions of the binary complex accumulate stresses around the binding interfaces between RNAP and DksA, and the ppGpp binding to the binary complex restores RNAP and DksA conformations to their original states (**Fig. 2, SMovies 1, 2 and 3**). Binding of ppGpp enhances DksA function by not only increasing its affinity for RNAP (**Fig. 5C**), but also by guiding the CC domain into a position that will effectively conflicts with the catalytic steps of RNA synthesis. Among the two ppGpp binding sites on RNAP, ppGpp binding at site 2 results in much larger effects on transcription inhibition as compared with the site 1, and the site 2 is formed only after DksA binds to RNAP (**Fig. 3**) (Ross et al., 2016). We therefore propose to re-evaluate the roles of DksA and ppGpp in their synergistic action on rRNA transcription inhibition as follows: DksA possesses the ability to influence RNAP activity and ppGpp allosterically potentiates activity of DksA. This is supported by studies of the structure

and function of TraR, including this study, showing that TraR possesses the same structural organization and mode of binding to RNAP as DksA, but influences RNAP transcriptions without requiring binding of ppGpp.

The structural basis for transcription inhibition by DksA/ppGpp and TraR

The structures and functions of DksA and TraR are similar. Both factors decrease transcription of ribosomal genes and increase transcription of amino acid biosynthesis genes (Blankschien et al., 2009b). The overall folds of DksA and TraR are remarkably similar (**Fig. 4B, SFigs. 1A and B**), despite TraR lacking the first 68 amino acids compared to DksA. These factors interact with RNAP in a similar manner (**Figs. 1 and 4**) by reaching into the active site via the elongated CC domain/NT-helix and contacting the DNA binding βlobe/i4 domain via the C-terminal CT-helix.

The *rrnB*P1 promoter is one of the strongest promoters in the *E. coli* genome and it has been investigated as a model promoter for understanding transcriptional regulation in response of changing growth conditions. Two major components have been implicated in the transcriptional regulation of this promoter, one inhibitory – mediated by DksA and ppGpp, and one stimulatory – mediated by the initiating nucleotide (iNTP) (Gaal et al., 1997; Paul et al., 2004; Perederina et al., 2004), which together explain the extreme magnitude of regulation at this promoter. DksA and ppGpp destabilize the RPo at the *rrnB*P1 promoter to the level that is below the detection limit *in vitro* and that allows for nearly complete shutdown of ribosomal transcription under nutrient starvation. When nutrients are replete and ppGpp levels decrease, the unstable RNAP–promoter complex shifts to the stable transcription-ready initiation complex in the presence of the initiating NTPs.

We modeled the transcription initiation complex with DksA by superposing the structures of the RNAP–DksA complex and the *de novo* transcription initiation complex (**Figs. 2A and B**) (Basu et al., 2014). In the absence of ppGpp, the CC tip of DksA does not occlude the iNTP binding site, however, it could interfere with NTP binding due to its acidic charges (**Fig. 2A**), consistent with the observation that the DksA increases the concentration of iNTP required to activate transcription from *rrnB*P1 (Doniselli et al., 2015; Paul et al., 2004). In the presence of ppGpp, the CC tip inserts deeply to the active site and denies iNTP access to the +2 NTP binding

site as well as prevents the folding of trigger loop (**Fig. 2B**), suggesting that it may repress the *rrnB*P1 transcription by direct inhibition of RNAP catalysis.

The βlobe/i4 domain interacts with the core recognition element (CRE) in the non-template DNA from -4 to +2 position, which is proposed to contribute to the formation and maintenance of the stable transcription bubble in the RPo (**SFig. 6A**) (Petushkov et al., 2015; Zhang et al., 2012). The contact between the CT-helix of DksA and the βlobe/i4 domain in the absence of ppGpp shifts the position of these domains relative to the main body of RNAP (**Fig. 2C, SMovie 1**) in a way that may weaken its grip on the non-template DNA in the transcription bubble and, therefore, decrease open complex stability. Consistent with this prediction, serial CT-helix truncations of DksA displayed a progressive loss of DksA function (Parshin et al., 2015). The importance of the βlobe/i4 domain for the DksA-dependent transcriptional repression is supported by isolation of Δ*dksA* suppressor mutations in the βlobe domain and also around linkers connecting the lobe domain to the main body of RNAP (Rutherford et al., 2009) (**SFig. 6A**).

Some Δ*dksA* suppressor mutations were also located at the switch regions of RNAP that serve as hinges of the RNAP clamp and undergo conformational changes during the opening and closing of the main channel in the course of the RPo formation (Feklistov et al., 2017; Srivastava et al., 2011). These suppressor mutations mimicked the negative effects of DksA on *rrnB*P1 transcription by not only inhibiting transcription but also by dramatically reducing RPo stability (Rutherford et al., 2009). In the crystal structures of RNAP determined in this study, the DNA binding channel is in the closed conformation, which has to be opened at the time of DNA loading into the channel (Feklistov et al., 2017). Although the association of DksA and ppGpp with RNAP does not influence the conformation of the DNA binding main channel (**Fig. 2E**), we speculate that the interaction between DksA and the βlobe/i4 domain may restrict opening of the main channel in the course of the RPo formation and, therefore, shift the dynamics in favor of the closed complex.

The binding of DksA to RNAP is similar to the binding of Gre factor to RNAP (**SFig. 7**). These factors insert their elongated CC domains to the secondary channel of RNAP and position the CC tip near the active site of RNAP. However, their influences on the structure of RNAP are different. The Gre factor binds and wraps around the edge of β'rim helix with the G domain but does not distort the structure of the β'rim helix. In addition, the Gre factor lacks a counterpart of

the CT-helix of DksA (**SFigs. 1A, B and C**), therefore it cannot influence the stability of the RPo via interaction with the βlobe/i4 domain.

ppGpp–DksA synergism effect during transcription inhibition

ppGpp increases the affinity of DksA for RNAP approximately 3-folds (**Fig. 5C**). In the absence of ppGpp, DksA binding to RNAP alters the conformations of the β'rim helix and DksA, resulting in destabilization of the RNAP–DksA complex. In the presence of ppGpp, DksA is reoriented such that it binds along the rim helix in a way that does not cause conformational distortions in RNAP or DksA and increases the contact area between the two proteins (**Fig. 2, SMovie 2**). The detrimental effects of the distortions in RNAP caused by DksA binding are further supported by the analysis of the TraR association with RNAP, which binds significantly tighter to RNAP than DksA in the absence of ppGpp (**Fig. 5B**) and does not alter the conformation of RNAP.

Amino acid substitutions in DksA, such as L15F and N88I, bypass the requirement for ppGpp in *E. coli* cells growing in nutrient depleted media. These DksA derivatives, known as super DksAs, increase the activity of the transcription factor and work independently of ppGpp (Blankschien et al., 2009a). Interestingly, these residues are not involved in binding to RNAP. Instead, these amino acids are located in the hydrophobic core of the G domain (L15) and in the center of the CC domain (N88); namely the areas of DksA that undergo large conformational changes during the RNAP–DksA binary complex formation (**SMovie 2**), These findings suggest that the amino acid substitutions may be involved in stabilization of a DksA conformation similar to that in the tertiary complex containing RNAP, DksA and ppGpp.

General model of transcription inhibitions by DksA and ppGpp

DksA and ppGpp effectively inhibit transcription from the *rrnB*P1 promoter in combination with the reduced concentrations of iNTPs during the stringent response, DksA and ppGpp effectively inhibit transcription from the *rrnB*P1 promoter. The structural information in this study provides a framework to explain the mechanism of synergistic action of DksA, ppGpp and iNTPs during transcription regulation.

Figure 6 shows three major steps in the course of transcription initiation from *rrnB*P1: promoter DNA binding by RNAP (step1), RPo formation (step 2), and formation of the

transcription initiation complex (RP_{INT}) (step 3). DksA can potentially bind and regulate transcription at any of these steps alone (scheme B) and with ppGpp (scheme C). Before DNA binding, the RNAP main channel holds the acidic and globular σ region 1.1 domain (Bae et al., 2013; Mekler et al., 2002; Murakami, 2013), which has to be ejected to load promoter DNA into the main channel and allow for the formation of RPo. In the step 2, the single-stranded template DNA has to pass through a barrier comprised of the σ finger (as known as σ region 3.2) located in front of the active site of RNAP (**SFig. 6A**), which later stabilizes the position of the template DNA (Basu et al., 2014; Zhang et al., 2012). Deletion of σ region 1.1 or 3.2 increases the half-life of the *rrnB*P1 RPo (Andrey Kulbachinsky, personal communication), suggesting that these domains negatively influence step 2.

The Steitz group determined the structure of the *E. coli* RNAP transcription initiation complex and showed that the β'i6 domain shifts its position toward the βlobe/i4 domain compared its position in the apo-form holoenzyme structure, resulting in closure of the gap between the β'jaw and βlobe/i4 domains (**SFig. 6C**) (Liu et al., 2016; Zuo and Steitz, 2015). These studies identified the structural basis for the formation of a stable RPo that involves the conformational change of the downstream mobile elements, including β'i6 and jaw domains, proposed by the Record group (Ruff et al., 2015a; Ruff et al., 2015b). Deletion of β'i6 drastically reduced the stability of the RPo (Artsimovitch et al., 2003), which is consistent with the idea that during closing, β'i6 may tighten the grip of RNAP on the downstream DNA (**SFig. 6C**). Moving β'i6 toward the βlobe/i4 domain eliminates the DksA binding site (**SFig. 6B**).

Prior to binding at the *rrnB*P1 promoter, RNAP holoenzyme can exist in 3 different forms in the presence of DksA and ppGpp including the apo-form (**A**), RNAP–DksA (**B**), and RNAP–DksA/ppGpp (**C**) (**Fig. 6**). The assembly of DksA with RNAP in scheme B is unstable, and it is further reduced in the promoter DNA complex (**Fig. 5E**), therefore, the RNAP–DksA complex without ppGpp likely forms transiently similar to the RNAP–GreB complex (Tetone et al., 2017) and does not have a significant impact on transcription from *rrnB*P1 unless a higher concentration of DksA is available, as in case of overproduction of DksA *in vivo* or addition of saturating amounts of DksA to *in vitro* experimental systems.

In contrast, after ppGpp binds at site 2 (scheme C), it enhances affinity of DksA for RNAP, not only for the apo-holoenzyme, but also for the RNAP–promoter complexes (**Figs. 5C and F**), as a consequence, DksA is able to effectively reduce the amount of RPo. Binding of

ppGpp also enhances the potency of DksA by excluding iNTP binding at the active site (**Fig. 2B**) and preventing trigger loop folding during the catalytic (step 3). The interaction between the CT-helix and the βlobe/i4 domain may lock it in a position that restricts the opening of main channel required for the RPo formation (step 2) (Feklistov et al., 2017). The stable association of DksA and ppGpp is likely to prevent closure of β'i6 during step 3 because of a steric clash with the G domain and CT-helix of DksA (**SFigs. 6B and C**).

ppGpp binding site 1

The DksA-independent ppGpp binding site 1 has been identified by crosslinking (Ross et al., 2013) and crystallographic studies of *E. coli* RNAP in complex with ppGpp (Mechold et al., 2013; Zuo et al., 2013). Although all the studies identified the same ppGpp binding site, the orientations of ppGpp proposed in the two crystallographic studies are different. Mechold *et al*. proposed that the 3'-diphosphate group of ppGpp is positioned near the β' subunit, whereas Zuo *et al*. assigned the same electron density to the guanine base in accordance with the cross-linking data (Ross et al., 2013). Experimental evidence compiled from the available structural and biochemical studies reveal the correct orientation of ppGpp at the site 1 as follows (**Fig. 3B**). The 5'- and 3'-phosphate groups face toward the ω subunit due to their larger electron densities compared with a conformation in which these groups are oriented toward the β' subunit. The 5'- and 3'-phosphate groups face the R3 and R52 residues of the ω subunit, respectively, can also be determined by comparing the structures of RNAP in complexes with ppGpp and pppGpp (Mechold et al., 2013). The guanine base faces the β' subunit, which is supported by the ^{32}P-6-thio-ppGpp crosslinks to β' subunit (Ross et al., 2013). In this orientation, His/Asp residues form hydrogen bonds with the guanine base, which explains the guanine base specific binding at the site 1.

Activation of Transcription by ppGpp and DksA

The structures described in this work provide straightforward models of how DksA alone and together with ppGpp block transcription initiation. However, DksA/ppGpp and TraR are also able to activate transcription at promoters such as those encoding genes for amino acid biosynthesis (Gopalkrishnan et al., 2017; Paul et al., 2005) and promoters regulated by the alternative σ^E factor (Gopalkrishnan et al., 2014). Mechanisms of transcription activation via

secondary channel binding proteins cannot be elucidated directly from the crystal structures determined in this study. Differences between the structures of DksA with and without ppGpp reveal the flexible nature of DksA's interaction with RNAP. Promoters that are positively regulated by DksA and ppGpp tend to form stable RPo suggesting that the mechanism of action involves distinct interactions with RNAP as compared to inhibition. Interestingly, DksA and ppGpp only activate and do not inhibit transcription by the holoenzyme containing σ^E, which is a member of the class 4 group of σ factors and has a reduced domain structure as compared to the primary σ factor, lacking region 1.1 and having shorter region 3.2, that are involved in sensitizing of *rrnB*P1 to regulation by DksA and ppGpp. Biochemical and structural studies with the σ^E holoenzyme in the absence and in the presence of DksA/ppGpp or TraR may better elucidate the basis for the activation since an inhibitory state is not accessible in this transcription system. Such experiments are underway.

EXPERIMENTAL PROCEDURES

Purification of σ^{70} RNAP holoenzymes

Expression, purification and reconstitution of wild-type and mutant *E. coli* σ^{70} RNAP holoenzymes were performed as previously described (Molodtsov et al., 2016).

Purification of DksA

A 3L culture containing BL21(DE3) cells transformed with a pSUMO–DksA vector, which contains *E. coli dksa* gene cloned to express a His_6-SUMO-DksA fusion, was grown in LB medium supplemented with 50 µg/ml Kanamycin and 200 µM $ZnCl_2$, induced with 1 mM IPTG at OD_{600} = 0.7, and protein expression was conducted for 3 hours at 30 °C. The cells were harvested by centrifugation and lysed by sonication in the lysis buffer (20 mM Tris-HCl, pH 8.0 at 4°C, 500 mM NaCl, 5% glycerol, 0.1 mM EDTA, 2 mM PMSF). The lysate was clarified by centrifugation for 30 min at 17,000 g, 4°C, and the supernatant was mixed with 1.5 ml of Ni agarose slurry (Qiagen) equilibrated with the lysis buffer and incubated on a shaker for 2 hours at 4 °C. The Ni resin was washed with 30 volumes of the lysis buffer followed by a 30 column volumes wash with the wash buffer (10 mM Tris-HCl, pH 8.0 at 4°C, 150 mM NaCl, 0.1 mM

EDTA) supplemented with 20 mM imidazole. Elution was carried using the wash buffer supplemented with 300 mM imidazole. The eluted protein was diluted with the wash buffer lacking NaCl to reduce the salt concentration to 70 mM and applied to a 1 ml sepharose Q column (GE Healthcare) equilibrated with the same buffer. SUMO–DksA was eluted by a linear gradient of 0.07-0.5 M NaCl over 40 column volumes. Fractions containing SUMO–DksA were diluted with the wash buffer lacking NaCl to reduce the salt concentration to 70 mM and incubated with UlpI protease to remove the SUMO tag overnight at 4°C. The sample was next mixed with 1.5 ml of equilibrated Ni agarose slurry (Qiagen), incubated on a shaker for 2 hours at 4°C, and centrifuged for 5 min at 6,000g, 4°C. The supernatant containing tag-less wild-type DksA was analyzed by SDS-PAGE and concentrated using VivaSpin concentrators. Aliquots of 1 mM DksA were frozen in liquid N_2 and stored at - 80°C until soaking to crystals.

Purification of TraR

A 3L cell culture of BL21(DE3) *E. coli* cells carrying pET24a-TraR-His6, pET24a vector with *E.coli traR* gene having a hexahistidine tag at the C-terminus (Blankschien et al., 2009b), was grown in LB medium supplemented with 200 µM $ZnCl_2$, induced with 1 mM IPTG at OD_{600} = 0.7, and protein expression was conducted for 3 hours at 30°C. The cells were harvested by centrifugation and lysed by sonication in the lysis buffer (20 mM Tris-HCl, pH 8.0 at 4°C, 500 mM NaCl, 5% glycerol, 0.1 mM EDTA, 2 mM PMSF). The lysate was clarified by centrifugation for 30 min at 17,000g, 4°C, and the supernatant was mixed with 1.5 ml of Ni agarose slurry (Qiagen) equilibrated with the lysis buffer and incubated on a shaker for 2 hours at 4°C. The Ni resin was washed with 30 volumes of the lysis buffer followed by a 30 column volumes wash with the wash buffer (10 mM Tris-HCl, pH 8.0 at 4°C, 150 mM NaCl, 0.1 mM EDTA) supplemented with 20 mM imidazole. Elution was carried using the wash buffer supplemented with 300 mM imidazole. The eluted protein was diluted with the wash buffer lacking NaCl to reduce the salt concentration to 70 mM and applied to a 1 ml sepharose Q column (GE Healthcare) equilibrated with the same buffer. TraR was eluted by a linear gradient of 0.07-0.5 M NaCl over 40 column volumes. Fractions containing TraR were analyzed by SDS-PAGE and concentrated using VivaSpin concentrators. Aliquots of 700 µM TraR were frozen in liquid N_2 and stored at - 80°C until soaking to crystals.

Crystallization of σ^{70} holoenzyme–DksA and TraR complexes

Crystallization of *E. coli* σ_{70} RNAP holoenzyme was performed as previously described (Murakami, 2013). To form co-crystals of RNAP and transcription factor, holoenzyme crystals were transferred to the cryoprotection solution (0.1 M HEPES (pH 7.0), 0.2 M calcium acetate, 25 % PEG400, 10 mM DTT) supplemented with 0.2 mM DksA or TraR and incubated overnight at 22 °C followed by flash-freezing in liquid N_2. To form crystals of RNAP–DksA/ppGpp, crystals soaked overnight with DksA were transferred to a fresh cryoprotection solution (0.1 M HEPES (pH 7.0), 0.02 M $MgCl_2$, 25% PEG400, 10 mM DTT) supplemented with 1 mM ppGpp and 0.05 mM DksA, incubated for 2 hours, and then flash-frozen in liquid N_2.

X-ray crystallographic data collection

The crystallographic datasets were collected at the Macromolecular Diffraction at the Cornell High Energy Synchrotron Source (MacCHESS) (Cornell University, Ithaca, NY) and the data were processed by HKL2000 (Otwinowski and Minor, 1997). The resolution limits for crystallographic datasets were determined based on completeness (>80 %) and $CC_{1/2}$ (>20 %) rather than R_{merge} and $\langle I \rangle/\sigma I > 2$ criteria, since this approach prevents loss of useful crystallographic data for structure refinement as found in a recent study (Karplus and Diederichs, 2012). The structures were solved by molecular replacement using the suite of programs PHENIX (Afonine et al., 2010) and *E. coli* RNAP holoenzyme (PDB: 4YG2) (Molodtsov et al., 2015) as a search model. Strong Fo-Fc maps corresponding to DksA, ppGpp and TraR were observed after the rigid body refinement. A crystal structure of DksA (Perederina et al., 2004), a homology model of TraR and ppGpp were fitted into these extra density maps to continue the refinement. The program Coot (Emsley and Cowtan, 2004) was used for manual adjustment of the models during refinement. A homology model of TraR was constructed by SWISS-MODEL (Biasini et al., 2014) using DksA (Perederina et al., 2004) and Zn-finger binding protein YBIL from *E. coli* (PDB: 2KGO) as reference structures. Final coordinates and structure factors were submitted to the PDB depository with ID codes listed in Table 1.

Fluorescence anisotropy assay

N-terminally His-tagged DksA-C35A was purified as previously described and stored in storage buffer (20 mM Tris-HCl (pH 8), 150 mM NaCl, 1 mM $ZnCl_2$ 10 mM 2-mercaptoethanol,

15% glycerol). Immediately before labeling, the storage buffer was exchanged by Bio-Gel P4 desalting column (Bio-Rad) equilibrated with a solution containing 50 mM HEPES (pH 7.4), 500 mM NaCl, 1 mM $ZnCl_2$, and 10% glycerol. Protein solution (10 µM) was then incubated on ice with sub-equimolar concentration of BODIPY-FL maleimide (Invitrogen/Molecular Probes) diluted from a 2.5 mM BODIPY-FL stock in DMSO. After 45 min of incubation, reaction was stopped by 10 mM 2-mercaptoethanol, unreacted dye was removed by using a Bio-Gel P4 desalting column equilibrated in a solution containing 50 mM Tris-HCl (pH 8), 500 mM NaCl, 1 mM $ZnCl_2$, and 10% glycerol twice. The degree of dye labeling was determined by measuring the absorbance of the labeled protein at 505 nm (ε_{505} = 79,000 M^{-1} cm^{-1}; ε_{280} = 1,300 M^{-1} cm^{-1}) and was typically > 50 %.

Double stranded promoter DNAs were annealed from corresponding oligonucleotides (**SFig. 7**). RNAP–promoter DNA complexes were assembled by incubation 2 µM RNAP and 12.5 µM corresponding DNA construct.

Direct anisotropy assays were performed with Corning black 384-well microplates with non-binding surface by using a microplate reader (Infinite M1000; Tecan) at 30 °C, with excitation at 470 nm and emission at 514 nm. Binding reaction mixtures (20 µl) containing 5 nM BODIPY FL-$DksA_{C35A}$ and 0 to 200 µM ppGpp and 0 to 1 µM RNAP (or RNAP–DNA complexes) in transcription buffer (50 mM Tris-HCl (pH 8), 10 mM $MgCl_2$, 50 mM NaCl, 5% glycerol, 10 mM 2-mercaptoethanol, 0.01% NP-40) were incubated at 37°C for 1 h, and anisotropy measurements were performed. The fractional occupancies were calculated as

$$\theta = (P - P_o) / (P_{max} - P_o) \quad (1)$$

where P_0 and P are polarization values before and after the addition of ligands, respectively, and P_{max} is the polarization value at saturation. Binding constants were obtained by fitting of the results to the Hill equation by non-linear regression using SigmaPlot.

Competition assays were used to determine the affinity of unlabeled DksA, TraR and DksA mutant derivatives for holo RNAP ($E\sigma^{70}$) and to determine the competition of DksA with promoter DNA. In these assays, reaction mixtures (20 µl) contained BODIPY FL-$DksA_{C35A}$, 100 nM RNAP, and either 0 or 50 µM ppGpp and 0 to 2 µM of unlabeled competitor proteins (e.g. TraR or DksA mutant) or promoter DNA duplexes. Components were incubated for 1 h at 37°C and fluorescence anisotropy was then measured. The 50% inhibitory concentrations (IC_{50}) were

calculated by using the Hill equation, and equilibrium dissociation constants (K_I) were calculated from the IC_{50} as follows, where K_D refers to the affinity of BODIPY FL-$DksA_{C35A}$ to RNAP (ref):

$K_I = IC_{50} / (1 + [RNAP] / K_D)$ (2)

Channel for NTP substrate entry analysis based on crystal structures of RNAP

To search for potential pathways for NTPs to enter from the protein surface to the active site, we adopted the program CAVER (Chovancova et al., 2012) to identify cavities in four static structures including apo-form holoenzyme (PDB: 4YG2), RNAP–DksA binary complex, RNAP–DksA/ppGpp ternary complex and RNAP–TraR complex. In our analysis, we followed previous studies (Batada et al., 2004; Zhang et al., 2015) to model the NTP molecule as a sphere of radius 3.5 Å, and adopted default input parameters in CAVER3.01 except for shell_radius=30 Å and shell_depth=50 Å (see (Chovancova et al., 2012) for details). For each structure, the averaged coordinates of the template DNA at +2 and +3 positions were chosen as the starting point for the pathway search in the main channel, while those of magnesium ion and +2 DNA were utilized for the secondary channel. We then identified the most probable pathway in both channels according to the available empty space and pathway distance (see (Chovancova et al., 2012) for methodology details).

Molecular models of NTP along the substrate entry pathways

We applied k-center clustering on all the points that constitute the pathways and divided them into 10 microstates according to their positions. The geometry center of each microstate was extracted as the reference position for modelling NTP along the pathways. The CTP was chosen to pair with the template DNA at +2 site and it coordinates with one magnesium ion. In particular, we aligned the center of mass of the CTP with Mg^{2+} to each microstate center and it was combined with the specific RNAP holoenzyme structure to build the model. We then solvated the whole complex in a dodecahedron water box and added enough sodium ions to neutralize the system. The size of the box was defined with box edges 1 Å away from the protein surface. We first froze protein and performed 5,000-steps energy minimization on the nucleic and NTP to let them re-orient to avoid the spatial clash. Afterwards, we put position restrain on all the heavy atoms of protein (with a force constant of 10 $kJ \cdot mol^{-1} \cdot Å^{-2}$) and carried out another

10,000-steps energy minimization for nucleic and NTP to make them further fit to their protein surroundings. Finally, the whole system was energy minimized for 10,000 steps to achieve the molecular model of NTP along the pathway. All energy minimizations were performed with Gromacs4.5 (Pronk et al., 2013). Amber99sb force field (Hornak et al., 2006) were used for the whole system with parameter modifications on the polyphosphate tail (Meagher et al., 2003) of NTP molecule.

AUTHOR CONTRIBUTIONS

V.M., S.E.A. and K.S.M. contributed to the design of the experiments and wrote the manuscript. V.M. prepared the crystals of RNAP in complex with DksA, DksA/ppGpp and TraR and collected the X-ray diffraction data, and K.S.M. determined their X-ray crystal structures. M.C. prepared ppGpp. L.Z. and X.H. analyzed the structures of RNAP to identify the NTP entry pathways to the active site. E.S. carried out the binding assay and analyzed the data with S.E.A. All authors discussed the results and commented on the manuscript.

ACKNOWLEDGEMENTS

We thank the staff at the CHESS/MacCHESS at Cornell University for support of crystallographic data collection. We thank Christophe Herman for providing the expression vector of TraR and thank Shoko Murakami for constructing pSUMO–DksA vector. We thank Andrey Kulbachinskiy, Irina Artsimovitch, Nikolay Zenkin, Sergei Borukhov, Vicky Shingler, Richard Gourse, Wilma Ross and Kasia Potrykus for critically reading the manuscript. This work was supported by NIH grants GM087350 (K.S.M.) and GM097365 (S.A.), and Hong Kong Research Grants Council HKUST C6009-15G (X.H.), and also funded in part by the Intramural Research Program, NIH (M.C.).

Table 1: Data collection and refinement statistics

RNAP complex with PDB code	**DksA** 5W1T	**DksA/ppGpp** 5VSW	**TraR** 5W1S
Data collection			
Space group	$P2_12_12_1$	$P2_12_12_1$	$P2_12_12_1$
Cell dimensions			
a (Å)	184.0	187.3	186.5
b (Å)	204.9	205.3	206.0
c (Å)	314.3	311.3	310.3
Resolution (Å)	50 – 4.5	50 – 4.3	50 – 3.8
Total reflections	474,850	531,876	911,081
Unique reflections	70,723	78,563	117,447
Redundancy	6.7 (5.7)	6.8 (6.4)	7.8 (7.4)
Completeness (%)	99.9 (99.9)	95.6 (95.3)	100.0 (100.0)
I / σ	16.6 (1.26)	12.2 (1.06)	17.5 (0.82)
Wilson B factor	199.4	187.8	156.5
R_{sym} (%)	10.0 (>100)	12.8 (>100)	9.2 (>100)
$CC^{1/2}$	(0.360)	(0.373)	(0.270)
Refinement			
Resolution (Å)	50 – 4.5	50 – 4.3	50 – 3.8
R_{work}	0.220	0.221	0.208
R_{free}	0.276	0.259	0.262
No. of atoms	58,066	57,643	56,825
B factors	291.6	279.0	239.0
R.m.s deviations			
Bond length (Å)	0.007	0.005	0.005
Bond angles (°)	1.147	1.08	1.068
Clashscore	16.8	17.2	17.6
Ramachandran favored, %	89.6	88.9	89.1
Ramachandran outliers, %	2.02	2.17	2.14

Data sets were collected at MacCHESS F1 line, Ithaca, NY
*Highest resolution shells are shown in parentheses

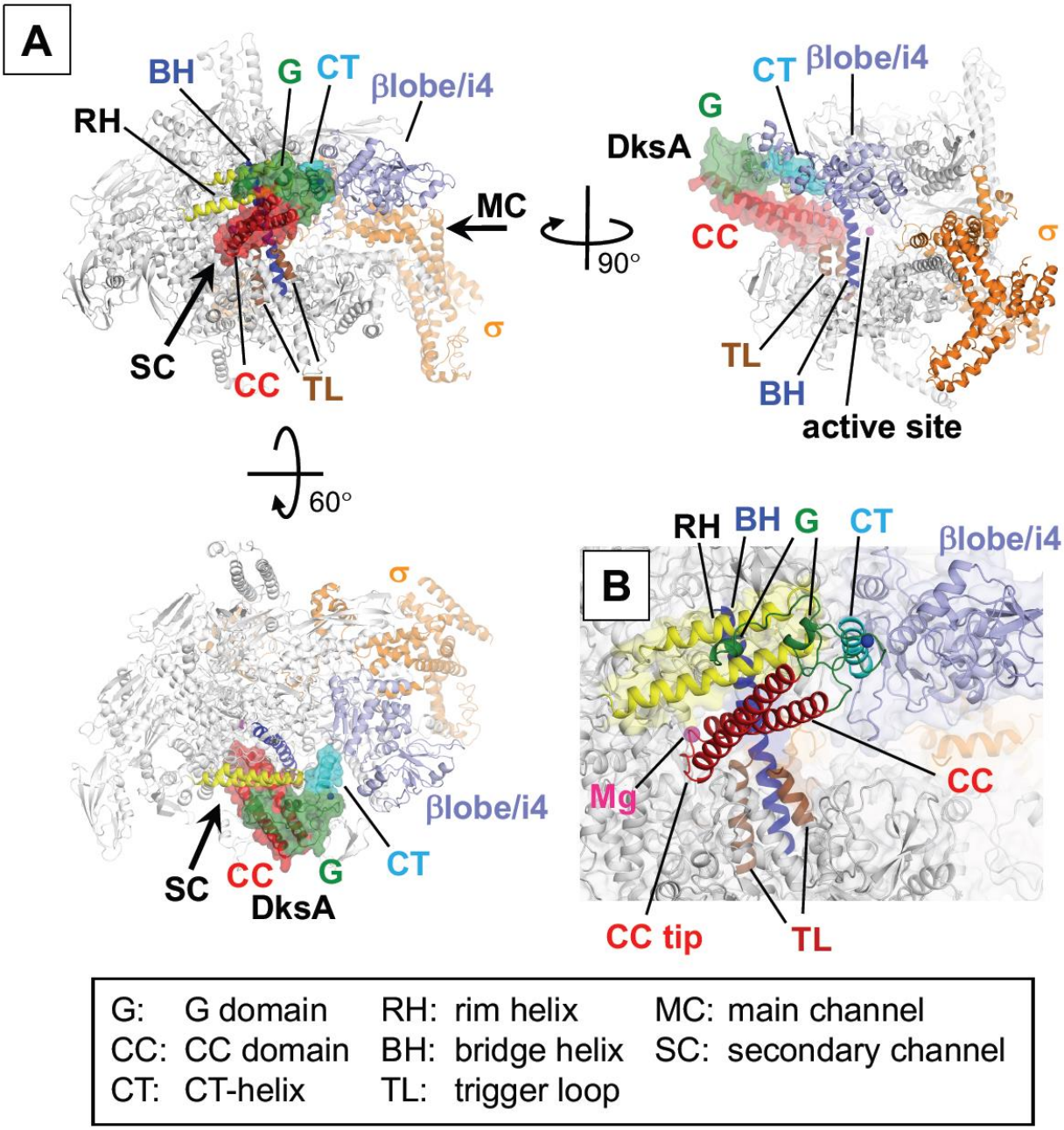

Figure 1. The structure of RNAP–DksA binary complex

(**A**) RNAP is depicted as ribbons and DksA is depicted as a ribbon with partially transparent surface. Relative orientations of the panels are indicated. Domains, motifs and regions of RNAP and DksA discussed in the text are labeled.

(**B**) A magnified view showing the RNAP and DksA interaction. Orientation of this panel is the same as in the left-top panel in **A**.

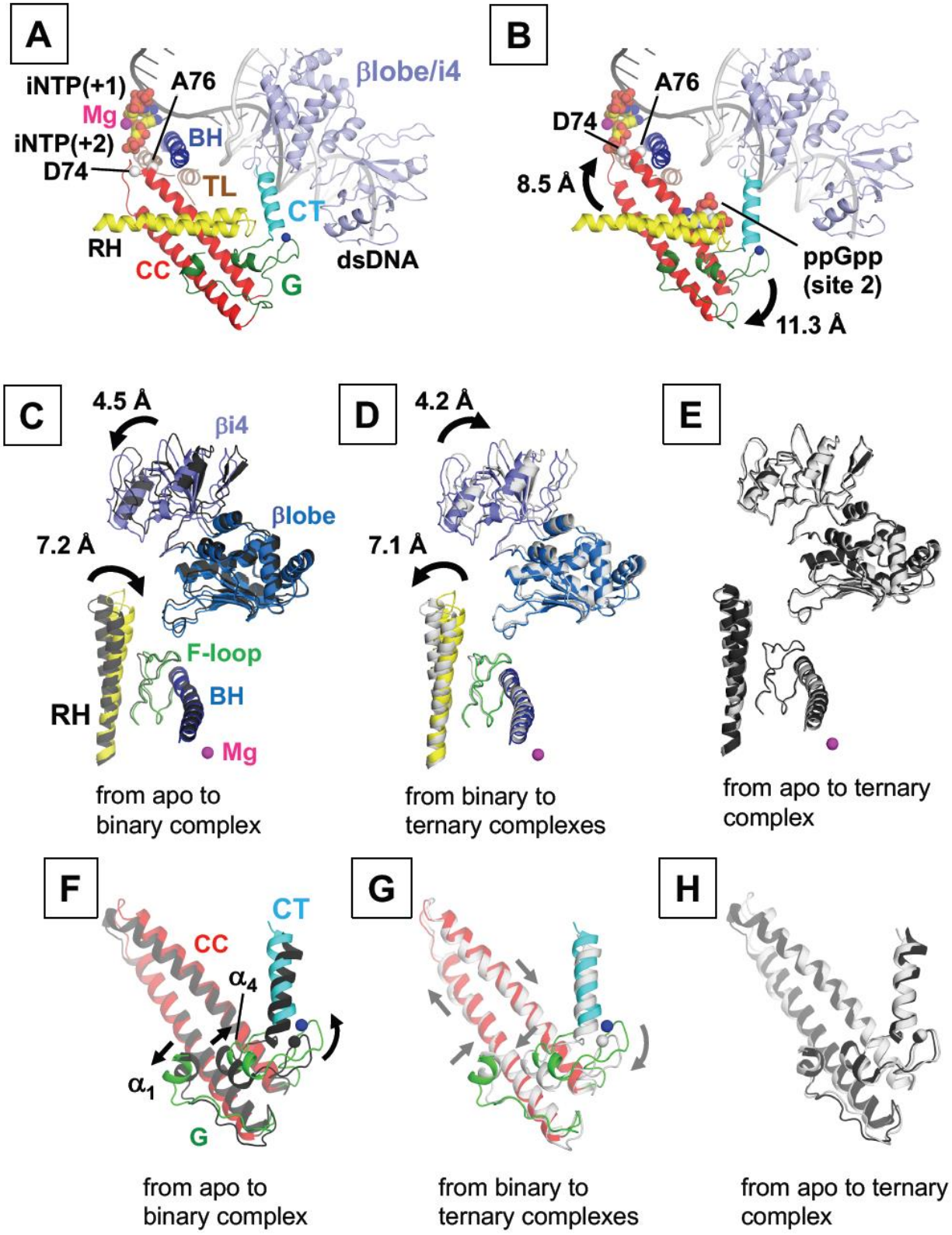
A
iNTP(+1)
Mg
iNTP(+2)
D74
A76
BH
TL
βlobe/i4
CT
RH
CC
G
dsDNA
B
A76
D74
8.5 Å
ppGpp
(site 2)
11.3 Å
C
4.5 Å
βi4
βlobe
7.2 Å
F-loop
BH
RH
Mg
from apo to
binary complex
D
4.2 Å
7.1 Å
from binary to
ternary complexes
E
from apo to ternary
complex
F
CT
CC
α4
α1
G
from apo to
binary complex
G
from binary to
ternary complexes
H
from apo to ternary
complex

Figure 2. The DksA and ppGpp bindings induce the conformation changes of RNAP and DksA

(**A-B**) Side-by-side comparison of DksA assembly with RNAP in the absence (**A**) and presence of ppGpp (**B**). RNAP and DksA are depicted as ribbons, and positions of D74 and A76 residues of DksA are indicated. ppGpp is shown as CPK representation in **B**. The DNA and iNTPs bound at +1 and +2 positions are modeled using *T. thermophilus* transcription initiation complex (PDB: 4Q4Z) (Basu et al., 2014). The rotations of DksA upon the ppGpp binding are indicated by arrows in **B**.

(**C-E**) RNAP conformational changes upon bindings of DksA (**C**) and ppGpp (**D**). The movements of the β'rim helix and βlobe/i4 domain are indicated by arrows. RNAP in the binary complex is depicted by color image, and RNAPs in the apo-form and in the ternary complex are shown as black and white ribbons, respectively. (**E**) Superimposed ribbon representation of RNAP between its apo-form (black) and in the ternary complex (white).

(**F-H**) DksA conformational changes upon binding to RNAP (**F**) and with ppGpp (**G**). The movements of DksA are indicated by arrows. DksA in the binary complex is depicted by the same color as in **A**, and DksA molecules in the apo-form and in the ternary complex are shown as black and white ribbons, respectively. (**H**) Superimposed ribbon representation of DksA in the apo-form (black) and in the ternary complex (white).

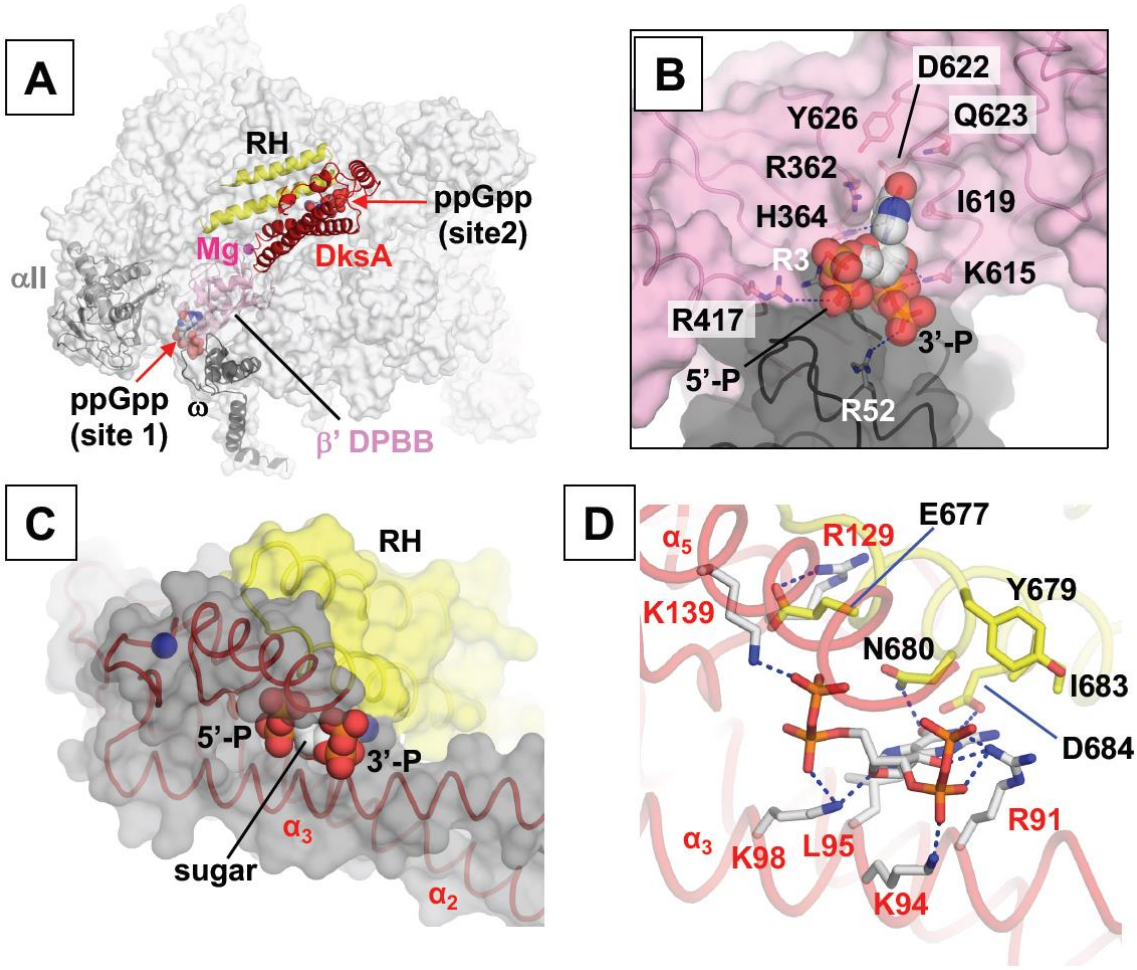

Figure 3. The ppGpp binding sites

(**A**) RNAP–DksA/ppGpp complex (RNAP: transparent white surface, DksA: red ribbon, ppGpp: CPK) shows the ppGpp binding sites 1 and 2. Domains and subunits of RNAP forming the ppGpp binding sites are shown as ribbon models and labeled.

(**B**) The ppGpp binding site 1. Amino acid residues (sticks) of β' and ω subunits involved in ppGpp binding are depicted as stick models on the ribbon and transparent surface models of β' (pink) and ω (dark gray) subunits. Amino acid residues are indicated (β': black, ω: white).

(**C**) The ppGpp binding site 2. DksA (gray surface and red ribbon), β'rim helix (yellow surface and ribbon) and ppGpp (CPK) are shown. Positions of the sugar and 5'- and 3'-phosphate groups of ppGpp are indicated.

(**D**) Amino acid residues of β' and DksA involved in ppGpp binding are depicted as stick models. Amino acid residues are indicated (β': black, DksA: red). The orientations of panels **C** and **D** are the same.

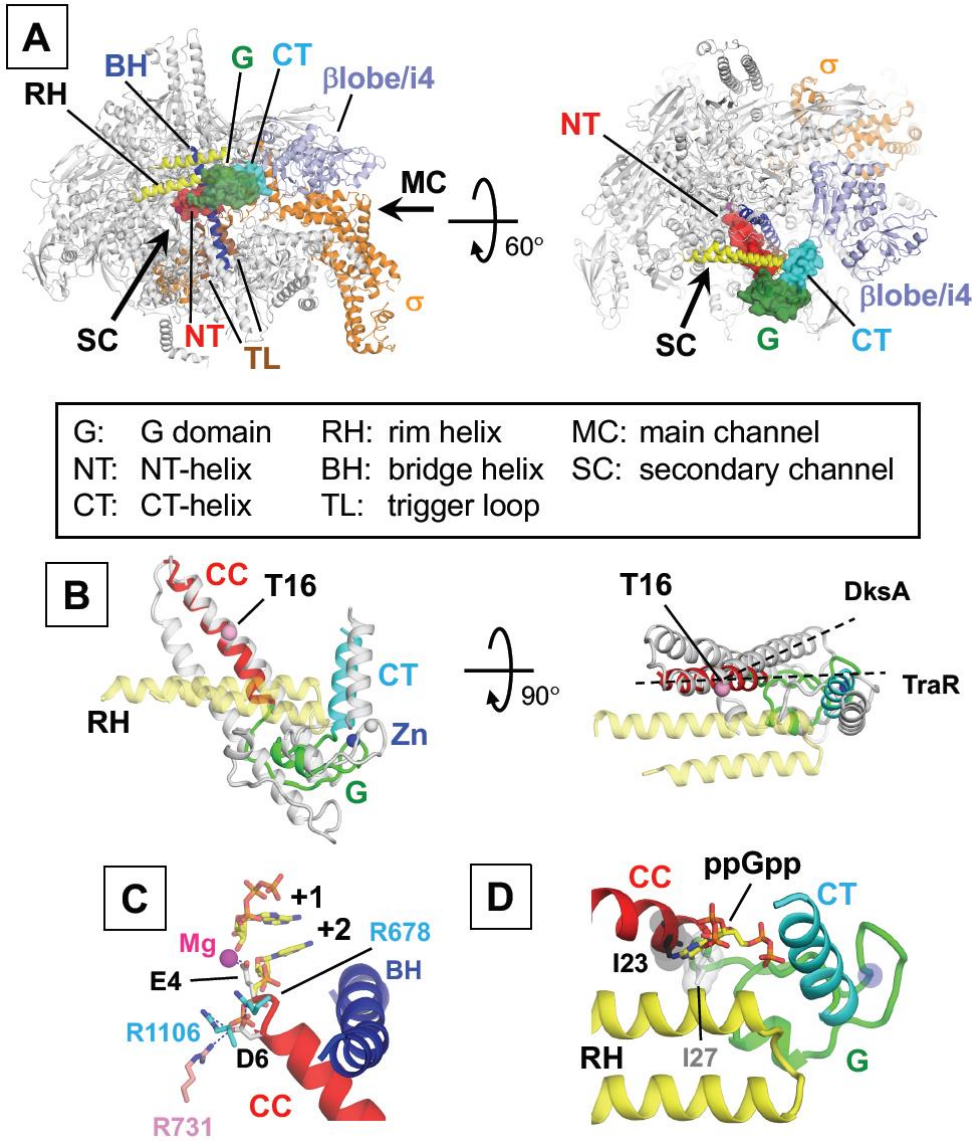

Figure 4. The RNAP and TraR complex

(**A**) RNAP is depicted as ribbons and TraR is depicted as a ribbon with partially transparent surface. The relative orientations of the panels are indicated.

(**B**) Comparison of the RNAP bound TraR (color image) and DksA (white). Positions of the N and C-terminus of TraR are indicated. The β'rim helix of RNAP is depicted as a partially transparent yellow ribbon model. The residue T16 of TraR (pink sphere) and the trajectories of α helixes of TraR and DksA interacting with the rim helix are depicted as black dashed lines.

(**C**) Interaction between the acidic residues of TraR (E4 and D6) and the RNAP active site (R678 and R1106 of β subunit; R731 of β' subunit). The model of iNTPs bound at the +1 and +2 positions are shown as stick models. The orientation of this panel is the same as the left panel of **B**.

(**D**) The ppGpp binding site 2 is occupied by hydrophobic residues of TraR (I23 and I27).

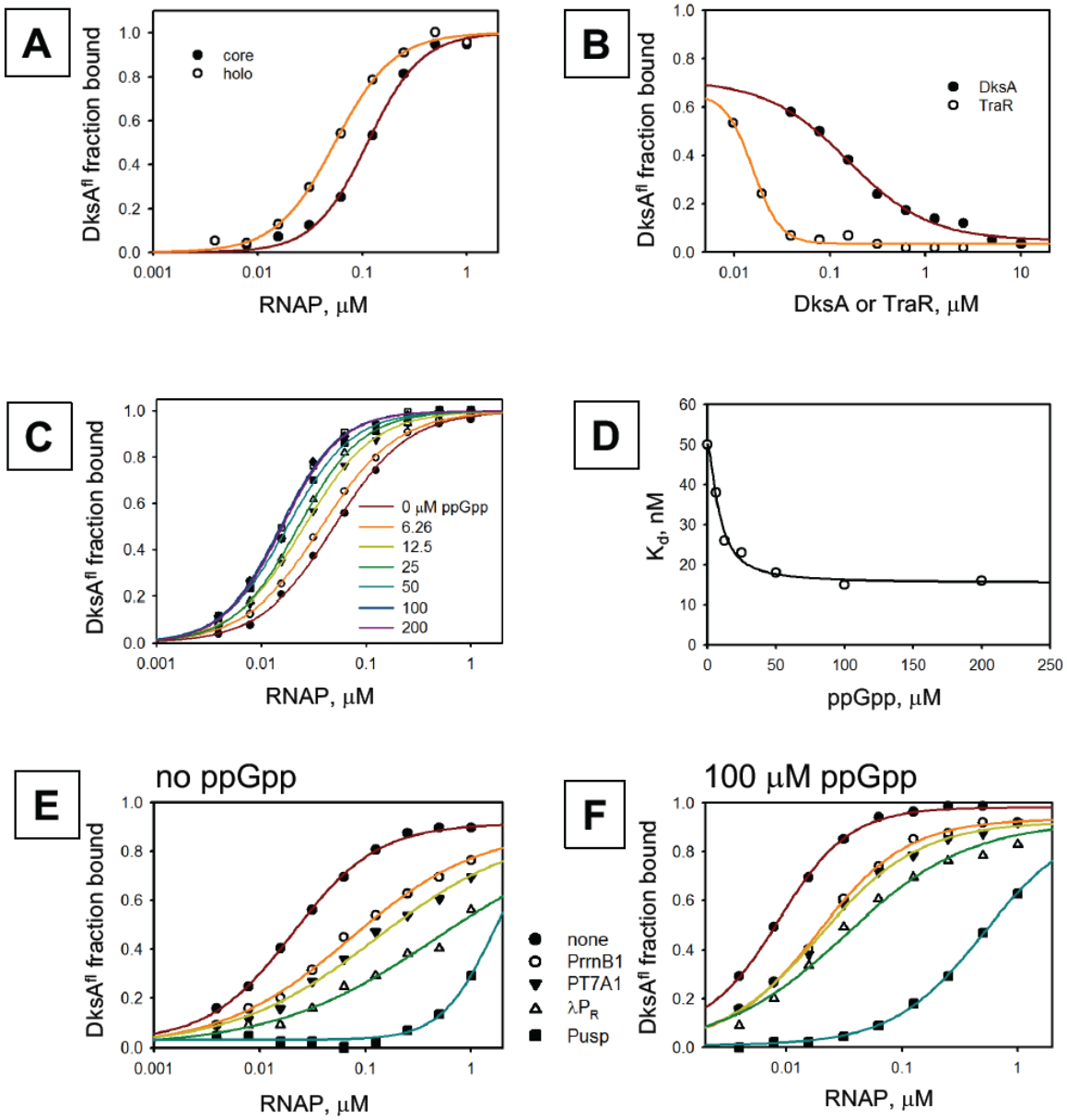

Figure 5. DksA affinities to RNAP in different forms as measured by the fluorescence anisotropy assay

(**A**) DksA^{fl} associations with RNAP in the absence of ppGpp.

(**B**) DksA and TraR competition with DksA^{fl} for RNAP holoenzyme binding in the absence of ppGpp.

(C-D) DksA^{fl} associations with RNAP holoenzyme in the different concentration of ppGpp.

(E-F) DksA binding to RNAP promoter DNA complex in the absence (**E**) and presence of ppGpp (**F**).

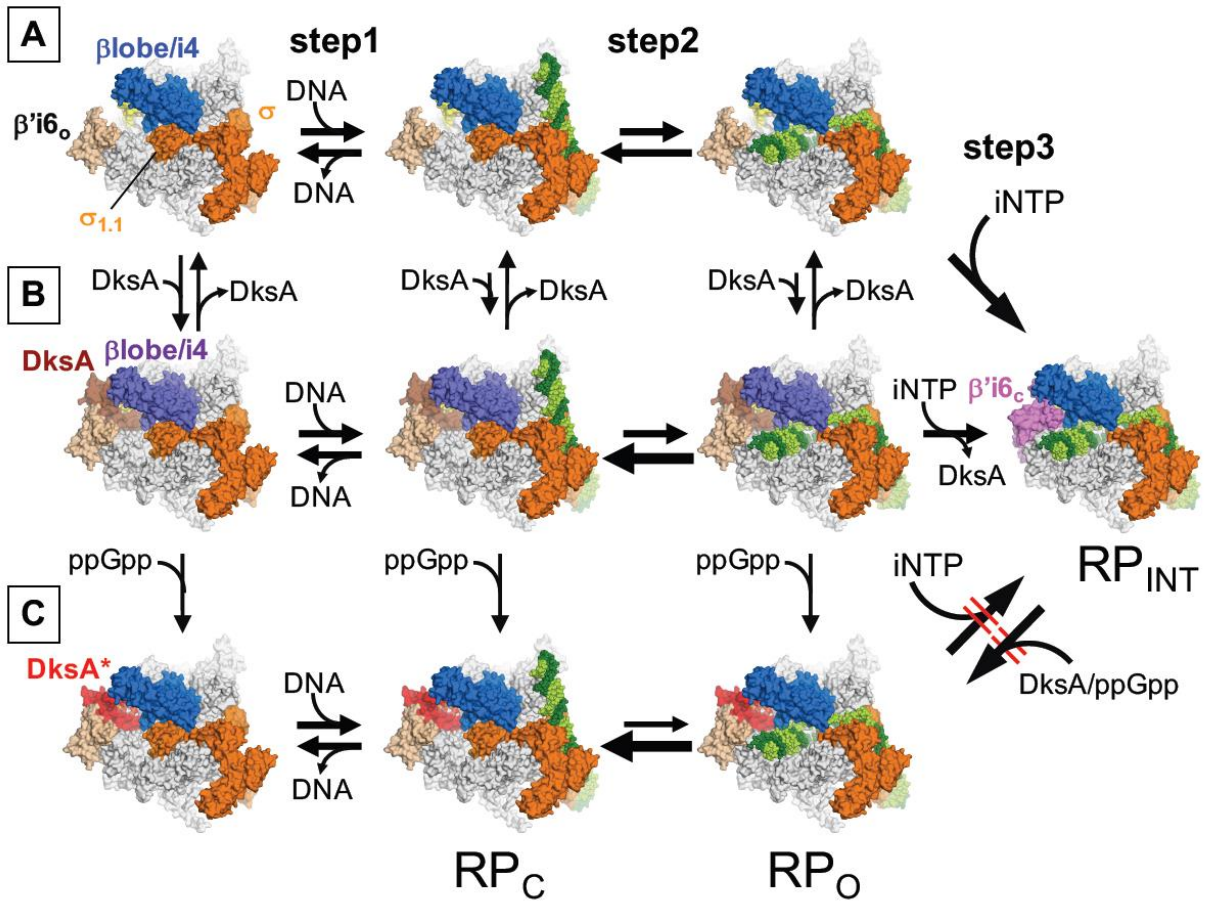

Figure 6. Three steps in the course of *rrnB*P1 transcription incorporated with DksA/ppGpp

RNAP and DksA are depicted as surface models (RNAP: white surface with colored key domains and the σ subunit; DksA: brown; DksA/ppGpp: red). The open ($\beta'i6_o$) and closed ($\beta'i6_c$) conformation of the β'i6 domains are indicated. DNA is shown as a CPK representation.

REFERENCES

Afonine, P.V., Mustyakimov, M., Grosse-Kunstleve, R.W., Moriarty, N.W., Langan, P., and Adams, P.D. (2010). Joint X-ray and neutron refinement with phenix.refine. Acta crystallographica Section D, Biological crystallography *66*, 1153-1163.

Artsimovitch, I., Svetlov, V., Murakami, K.S., and Landick, R. (2003). Co-overexpression of Escherichia coli RNA polymerase subunits allows isolation and analysis of mutant enzymes lacking lineage-specific sequence insertions. J Biol Chem *278*, 12344-12355.

Bae, B., Davis, E., Brown, D., Campbell, E.A., Wigneshweraraj, S., and Darst, S.A. (2013). Phage T7 Gp2 inhibition of Escherichia coli RNA polymerase involves misappropriation of sigma70 domain 1.1. Proc Natl Acad Sci U S A *110*, 19772-19777.

Basu, R.S., Warner, B.A., Molodtsov, V., Pupov, D., Esyunina, D., Fernandez-Tornero, C., Kulbachinskiy, A., and Murakami, K.S. (2014). Structural basis of transcription initiation by bacterial RNA polymerase holoenzyme. J Biol Chem *289*, 24549-24559.

Batada, N.N., Westover, K.D., Bushnell, D.A., Levitt, M., and Kornberg, R.D. (2004). Diffusion of nucleoside triphosphates and role of the entry site to the RNA polymerase II active center. Proc Natl Acad Sci U S A *101*, 17361-17364.

Biasini, M., Bienert, S., Waterhouse, A., Arnold, K., Studer, G., Schmidt, T., Kiefer, F., Gallo Cassarino, T., Bertoni, M., Bordoli, L., *et al.* (2014). SWISS-MODEL: modelling protein tertiary and quaternary structure using evolutionary information. Nucleic acids research *42*, W252-258.

Blankschien, M.D., Lee, J.H., Grace, E.D., Lennon, C.W., Halliday, J.A., Ross, W., Gourse, R.L., and Herman, C. (2009a). Super DksAs: substitutions in DksA enhancing its effects on transcription initiation. EMBO J *28*, 1720-1731.

Blankschien, M.D., Potrykus, K., Grace, E., Choudhary, A., Vinella, D., Cashel, M., and Herman, C. (2009b). TraR, a homolog of a RNAP secondary channel interactor, modulates transcription. PLoS Genet *5*, e1000345.

Cashel, M., and Gallant, J. (1969). Two compounds implicated in the function of the RC gene of Escherichia coli. Nature *221*, 838-841.

Chlenov, M., Masuda, S., Murakami, K.S., Nikiforov, V., Darst, S.A., and Mustaev, A. (2005). Structure and function of lineage-specific sequence insertions in the bacterial RNA polymerase beta' subunit. J Mol Biol *353*, 138-154.

Chovancova, E., Pavelka, A., Benes, P., Strnad, O., Brezovsky, J., Kozlikova, B., Gora, A., Sustr, V., Klvana, M., Medek, P., *et al.* (2012). CAVER 3.0: A Tool for the Analysis of Transport Pathways in Dynamic Protein Structures. Plos Computational Biology *8*, e1002708.

Dalebroux, Z.D., and Swanson, M.S. (2012). ppGpp: magic beyond RNA polymerase. Nat Rev Microbiol *10*, 203-212.

Doniselli, N., Rodriguez-Aliaga, P., Amidani, D., Bardales, J.A., Bustamante, C., Guerra, D.G., and Rivetti, C. (2015). New insights into the regulatory mechanisms of ppGpp and DksA on Escherichia coli RNA polymerase-promoter complex. Nucleic acids research *43*, 5249-5262.

Durfee, T., Hansen, A.M., Zhi, H., Blattner, F.R., and Jin, D.J. (2008). Transcription profiling of the stringent response in Escherichia coli. Journal of bacteriology *190*, 1084-1096.

Emsley, P., and Cowtan, K. (2004). Coot: model-building tools for molecular graphics. Acta crystallographica Section D, Biological crystallography *60*, 2126-2132.

Feklistov, A., Bae, B., Hauver, J., Lass-Napiorkowska, A., Kalesse, M., Glaus, F., Altmann, K.H., Heyduk, T., Landick, R., and Darst, S.A. (2017). RNA polymerase motions during promoter melting. Science *356*, 863-866.

Gaal, T., Bartlett, M.S., Ross, W., Turnbough, C.L., Jr., and Gourse, R.L. (1997). Transcription regulation by initiating NTP concentration: rRNA synthesis in bacteria. Science *278*, 2092-2097.

Gentry, D., Xiao, H., Burgess, R., and Cashel, M. (1991). The omega subunit of Escherichia coli K-12 RNA polymerase is not required for stringent RNA control in vivo. Journal of bacteriology *173*, 3901-3903.

Gopalkrishnan, S., Nicoloff, H., and Ades, S.E. (2014). Co-ordinated regulation of the extracytoplasmic stress factor, sigmaE, with other Escherichia coli sigma factors by (p)ppGpp and DksA may be achieved by specific regulation of individual holoenzymes. Mol Microbiol *93*, 479-493.

Gopalkrishnan, S., Ross, W., Chen, A.Y., and Gourse, R.L. (2017). TraR directly regulates transcription initiation by mimicking the combined effects of the global regulators DksA and ppGpp. Proc Natl Acad Sci U S A *114*, E5539-E5548.

Grace, E.D., Gopalkrishnan, S., Girard, M.E., Blankschien, M.D., Ross, W., Gourse, R.L., and Herman, C. (2015). Activation of the sigmaE-dependent stress pathway by conjugative TraR may anticipate conjugational stress. J Bacteriol *197*, 924-931.

Gummesson, B., Lovmar, M., and Nystrom, T. (2013). A proximal promoter element required for positive transcriptional control by guanosine tetraphosphate and DksA protein during the stringent response. J Biol Chem *288*, 21055-21064.

Haugen, S.P., Ross, W., and Gourse, R.L. (2008). Advances in bacterial promoter recognition and its control by factors that do not bind DNA. Nat Rev Microbiol *6*, 507-519.

Hauryliuk, V., Atkinson, G.C., Murakami, K.S., Tenson, T., and Gerdes, K. (2015). Recent functional insights into the role of (p)ppGpp in bacterial physiology. Nat Rev Microbiol *13*, 298-309.

Hornak, V., Abel, R., Okur, A., Strockbine, B., Roitberg, A., and Simmerling, C. (2006). Comparison of multiple amber force fields and development of improved protein backbone parameters. Proteins *65*, 712-725.

Igarashi, K., Fujita, N., and Ishihama, A. (1989). Promoter selectivity of Escherichia coli RNA polymerase: omega factor is responsible for the ppGpp sensitivity. Nucleic acids research *17*, 8755-8765.

Karplus, P.A., and Diederichs, K. (2012). Linking crystallographic model and data quality. Science *336*, 1030-1033.

Kettenberger, H., Armache, K.J., and Cramer, P. (2003). Architecture of the RNA polymerase II-TFIIS complex and implications for mRNA cleavage. Cell *114*, 347-357.

Lee, J.H., Lennon, C.W., Ross, W., and Gourse, R.L. (2012). Role of the coiled-coil tip of Escherichia coli DksA in promoter control. J Mol Biol *416*, 503-517.

Lennon, C.W., Gaal, T., Ross, W., and Gourse, R.L. (2009). Escherichia coli DksA binds to Free RNA polymerase with higher affinity than to RNA polymerase in an open complex. Journal of bacteriology *191*, 5854-5858.

Liu, B., Zuo, Y., and Steitz, T.A. (2016). Structures of E. coli sigmaS-transcription initiation complexes provide new insights into polymerase mechanism. Proc Natl Acad Sci U S A *113*, 4051-4056.

Lyzen, R., Kochanowska, M., Wegrzyn, G., and Szalewska-Palasz, A. (2009). Transcription from bacteriophage lambda pR promoter is regulated independently and antagonistically by DksA and ppGpp. Nucleic acids research *37*, 6655-6664.

Maneewannakul, K., and Ippen-Ihler, K. (1993). Construction and analysis of F plasmid traR, trbJ, and trbH mutants. Journal of bacteriology *175*, 1528-1531.

Meagher, K.L., Redman, L.T., and Carlson, H.A. (2003). Development of polyphosphate parameters for use with the AMBER force field. J Comput Chem *24*, 1016-1025.

Mechold, U., Potrykus, K., Murphy, H., Murakami, K.S., and Cashel, M. (2013). Differential regulation by ppGpp versus pppGpp in Escherichia coli. Nucleic acids research *41*, 6175-6189.

Mekler, V., Kortkhonjia, E., Mukhopadhyay, J., Knight, J., Revyakin, A., Kapanidis, A.N., Niu, W., Ebright, Y.W., Levy, R., and Ebright, R.H. (2002). Structural organization of bacterial RNA polymerase holoenzyme and the RNA polymerase-promoter open complex. Cell *108*, 599-614.

Molodtsov, V., Fleming, P.R., Eyermann, C.J., Ferguson, A.D., Foulk, M.A., McKinney, D.C., Masse, C.E., Buurman, E.T., and Murakami, K.S. (2015). X-ray crystal structures of Escherichia coli RNA polymerase with switch region binding inhibitors enable rational design of squaramides with an improved fraction unbound to human plasma protein. J Med Chem *58*, 3156-3171.

Molodtsov, V., Scharf, N.T., Stefan, M.A., Garcia, G.A., and Murakami, K.S. (2016). Structural basis for rifamycin resistance of bacterial RNA polymerase by the three most clinically important RpoB mutations found in Mycobacterium tuberculosis. Mol Microbiol, Epub ahead of print.

Murakami, K.S. (2013). The X-ray crystal structure of Escherichia coli RNA polymerase σ70 holoenzyme. The Journal of biological chemistry *288*, 9126-9134.

Opalka, N., Chlenov, M., Chacon, P., Rice, W.J., Wriggers, W., and Darst, S.A. (2003). Structure and function of the transcription elongation factor GreB bound to bacterial RNA polymerase. Cell *114*, 335-345.

Otwinowski, Z., and Minor, W. (1997). Processing of X-ray diffraction data collected in oscillation mode. Methods Enzymol *276*, 307-326.

Parshin, A., Shiver, A.L., Lee, J., Ozerova, M., Schneidman-Duhovny, D., Gross, C.A., and Borukhov, S. (2015). DksA regulates RNA polymerase in Escherichia coli through a network of interactions in the secondary channel that includes Sequence Insertion 1. Proc Natl Acad Sci U S A *112*, E6862-6871.

Paul, B.J., Barker, M.M., Ross, W., Schneider, D.A., Webb, C., Foster, J.W., and Gourse, R.L. (2004). DksA: a critical component of the transcription initiation machinery that potentiates the regulation of rRNA promoters by ppGpp and the initiating NTP. Cell *118*, 311-322.

Paul, B.J., Berkmen, M.B., and Gourse, R.L. (2005). DksA potentiates direct activation of amino acid promoters by ppGpp. Proc Natl Acad Sci U S A *102*, 7823-7828.

Perederina, A., Svetlov, V., Vassylyeva, M.N., Tahirov, T.H., Yokoyama, S., Artsimovitch, I., and Vassylyev, D.G. (2004). Regulation through the secondary channel--structural framework for ppGpp-DksA synergism during transcription. Cell *118*, 297-309.

Petushkov, I., Pupov, D., Bass, I., and Kulbachinskiy, A. (2015). Mutations in the CRE pocket of bacterial RNA polymerase affect multiple steps of transcription. Nucleic acids research *43*, 5798-5809.

Potrykus, K., and Cashel, M. (2008). (p)ppGpp: still magical? Annu Rev Microbiol *62*, 35-51.

Pronk, S., Pall, S., Schulz, R., Larsson, P., Bjelkmar, P., Apostolov, R., Shirts, M.R., Smith, J.C., Kasson, P.M., van der Spoel, D., *et al.* (2013). GROMACS 4.5: a high-throughput and highly parallel open source molecular simulation toolkit. Bioinformatics *29*, 845-854.

Ross, W., Sanchez-Vazquez, P., Chen, A.Y., Lee, J.H., Burgos, H.L., and Gourse, R.L. (2016). ppGpp Binding to a Site at the RNAP-DksA Interface Accounts for Its Dramatic Effects on Transcription Initiation during the Stringent Response. Molecular cell *62*, 811-823.

Ross, W., Vrentas, C.E., Sanchez-Vazquez, P., Gaal, T., and Gourse, R.L. (2013). The magic spot: a ppGpp binding site on E. coli RNA polymerase responsible for regulation of transcription initiation. Molecular cell *50*, 420-429.

Ruff, E.F., Drennan, A.C., Capp, M.W., Poulos, M.A., Artsimovitch, I., and Record, M.T., Jr. (2015a). E. coli RNA Polymerase Determinants of Open Complex Lifetime and Structure. J Mol Biol *427*, 2435-2450.

Ruff, E.F., Record, M.T., Jr., and Artsimovitch, I. (2015b). Initial events in bacterial transcription initiation. Biomolecules *5*, 1035-1062.

Rutherford, S.T., Lemke, J.J., Vrentas, C.E., Gaal, T., Ross, W., and Gourse, R.L. (2007). Effects of DksA, GreA, and GreB on transcription initiation: insights into the mechanisms of factors that bind in the secondary channel of RNA polymerase. J Mol Biol *366*, 1243-1257.

Rutherford, S.T., Villers, C.L., Lee, J.H., Ross, W., and Gourse, R.L. (2009). Allosteric control of Escherichia coli rRNA promoter complexes by DksA. Genes Dev *23*, 236-248.

Sekine, S., Murayama, Y., Svetlov, V., Nudler, E., and Yokoyama, S. (2015). The ratcheted and ratchetable structural states of RNA polymerase underlie multiple transcriptional functions. Molecular cell *57*, 408-421.

Srivastava, A., Talaue, M., Liu, S., Degen, D., Ebright, R.Y., Sineva, E., Chakraborty, A., Druzhinin, S.Y., Chatterjee, S., Mukhopadhyay, J., *et al.* (2011). New target for inhibition of bacterial RNA polymerase: 'switch region'. Curr Opin Microbiol *14*, 532-543.

Tagami, S., Sekine, S., Kumarevel, T., Hino, N., Murayama, Y., Kamegamori, S., Yamamoto, M., Sakamoto, K., and Yokoyama, S. (2010). Crystal structure of bacterial RNA polymerase bound with a transcription inhibitor protein. Nature *468*, 978-982.

Tetone, L.E., Friedman, L.J., Osborne, M.L., Ravi, H., Kyzer, S., Stumper, S.K., Mooney, R.A., Landick, R., and Gelles, J. (2017). Dynamics of GreB-RNA polymerase interaction allow a proofreading accessory protein to patrol for transcription complexes needing rescue. Proc Natl Acad Sci U S A *114*, E1081-E1090.

Yuzenkova, Y., Bochkareva, A., Tadigotla, V.R., Roghanian, M., Zorov, S., Severinov, K., and Zenkin, N. (2010). Stepwise mechanism for transcription fidelity. BMC Biol *8*, 54.

Zhang, J., Palangat, M., and Landick, R. (2010). Role of the RNA polymerase trigger loop in catalysis and pausing. Nat Struct Mol Biol *17*, 99-104.

Zhang, L., Silva, D.-A., Pardo-Avila, F., Wang, D., and Huang, X. (2015). Structural Model of RNA Polymerase II Elongation Complex with Complete Transcription Bubble Reveals NTP Entry Routes. PLoS Comput Biol *11*, e1004354.

Zhang, Y., Feng, Y., Chatterjee, S., Tuske, S., Ho, M.X., Arnold, E., and Ebright, R.H. (2012). Structural basis of transcription initiation. Science *338*, 1076-1080.

Zuo, Y., and Steitz, T.A. (2015). Crystal structures of the *E. coli* transcription initiation complexes with a complete bubble. Molecular cell *58*, 534-540.

Zuo, Y., Wang, Y., and Steitz, T.A. (2013). The mechanism of E. coli RNA polymerase regulation by ppGpp is suggested by the structure of their complex. Molecular cell *50*, 430-436.

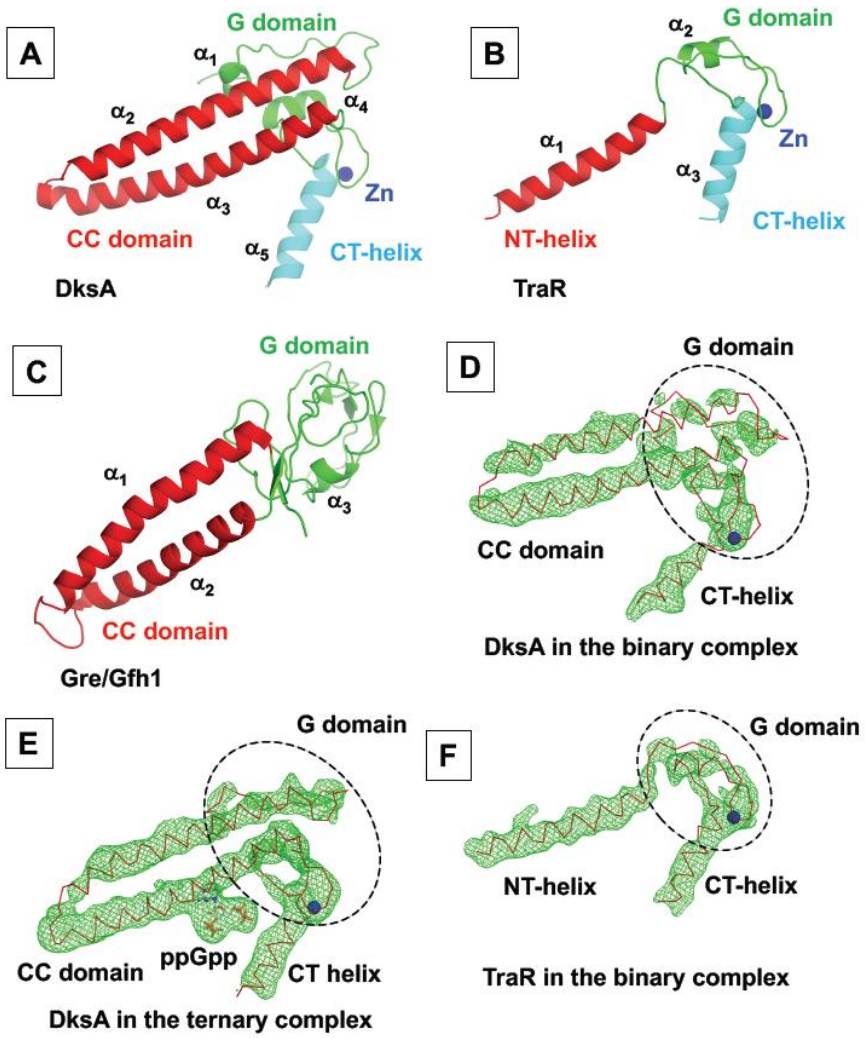

Supplemental Figure 1. Structures of DksA, TraR and Gre/Gfh1 and *Fo–Fc* density maps showing DksA, DksA/ppGpp and TraR in their complexes with RNAP

(**A-C**) The crystal structures of apo-form DksA (PDB: 1TLJ, molecule A) (**A**), TraR in the RNAP–TraR complex (PDB: 5W1S) (**B**) and Gre/Gfh1 chimera in the RNAP–Gre/Gfh1 complex (PDB: 4WQT) (**C**). Structural parts of these factors and positions of α helixes are indicated. (**D-F**) *Fo–Fc* electron density maps (green mesh, σ=3) of the DksA in the binary (**D**) and ternary complexes (**E**) and the TraR in the RNAP–TraR complex (**F**). DksA and TraR are shown as red backbone ribbons, Zn atoms in their Zn binding site are blue sphere and ppGpp is depicted as a stick model. Three structural parts of DksA and TraR are indicated.

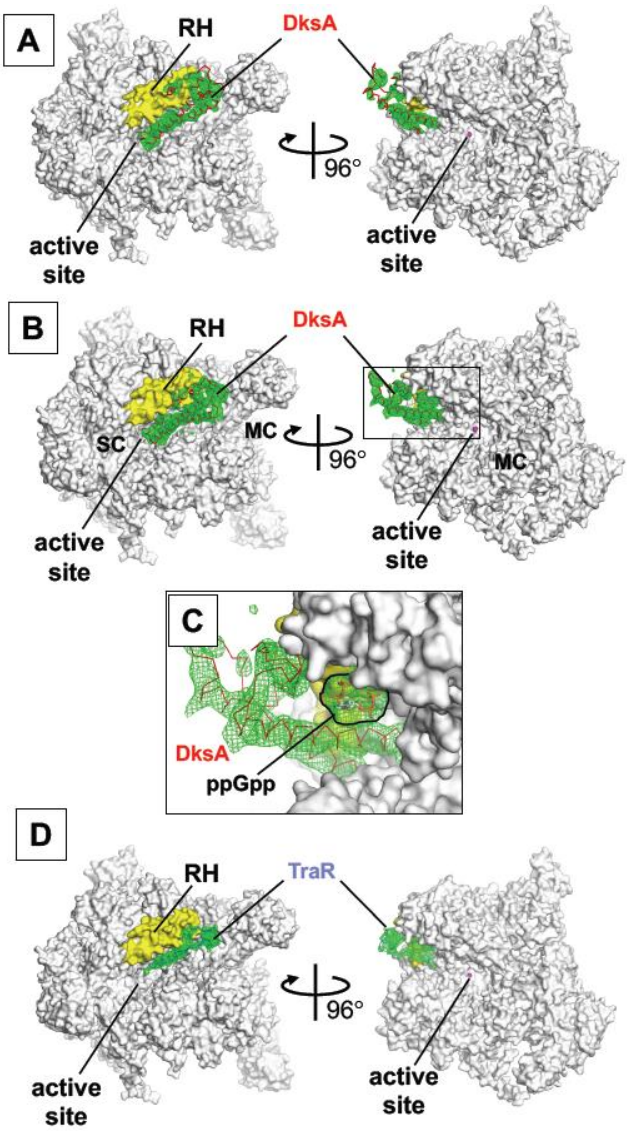

Supplemental Figure 2. *Fo–Fc* density maps showing DksA, DksA/ppGpp and TraR in their complexes with RNAP

E. coli RNAP holoenzyme is depicted as molecular surface (white) with the active site Mg (magenta sphere) and β'rim helix (yellow) shown in colors. *Fo–Fc* electron density maps (σ=3) of RNAP–DksA (**A**) and RNAP–DksA/ppGpp (**B**) complexes phased with the holoenzyme are shown as green meshes. The DksA is shown as red backbone ribbon and ppGpp is depicted as stick model. The right and left panels show the main channel (MC) and the secondary channel (SC) of RNAP in their middles, respectively. (**C**) A magnified view of the boxed region in **B**, showing a *Fo–Fc* map corresponding to ppGpp (outlined by black). (**D**) *E. coli* RNAP holoenzyme is depicted as molecular surface (white) with the active site Mg (magenta sphere) and β'rim helix (yellow) shown in colors. *Fo–Fc* electron density maps (σ=3) of the RNAP–TraR complex phased with the holoenzyme are shown as green meshes. TraR is shown as a backbone ribbon.

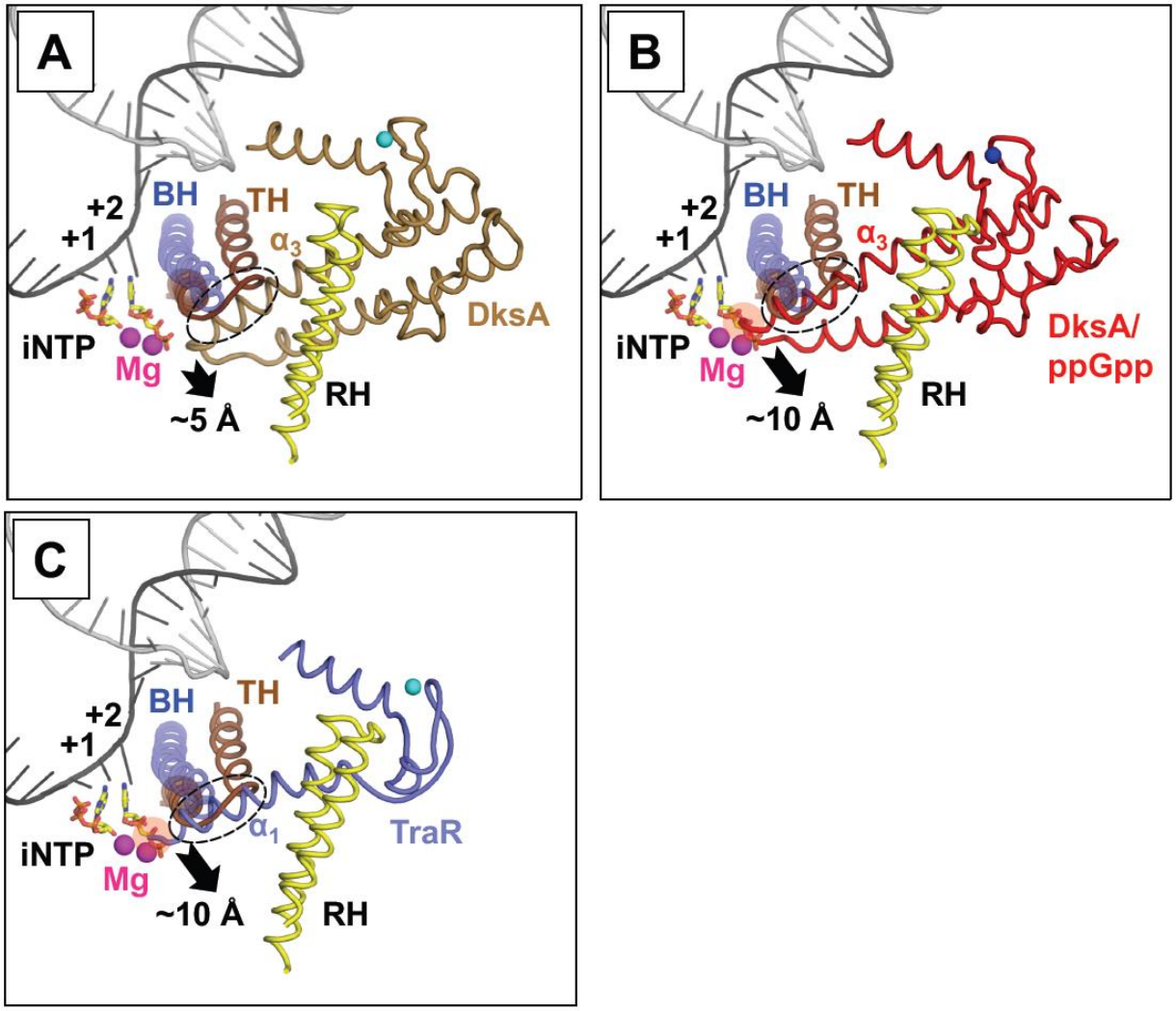

Supplemental Figure 3. The acidic tips of DksA and TraR restrict trigger loop folding and the iNTP binding at +2 position

DksA and TraR are depicted as ribbon models in (**A**) the RNAP–DksA complex, (**B**) the RNAP–DksA/ppGpp complex and (**C**) the RNAP–TraR complex. The β'rim helix and bridge helix of RNAP are also depicted. The folded trigger loop, the trigger helix (TH), is modeled from the *T. thermophilus* transcription elongation complex (PDB: 2O5J), while the DNA and iNTPs are modeled using the *T. thermophilus* transcription initiation complex (PDB: 4Q4Z). Movements of the CC tip of DksA and the NT-helix of TraR required for folding the TH are indicated by arrows.

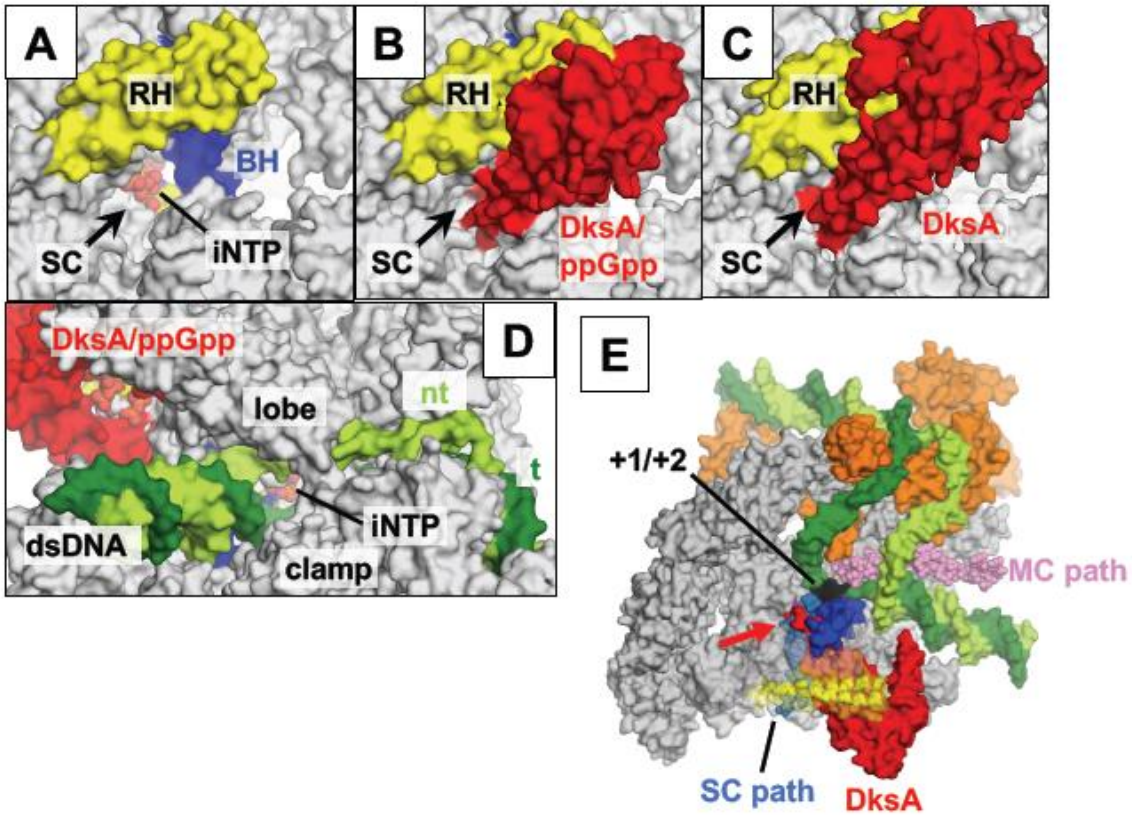

Supplemental Figure 4. RNAP and DksA interaction and the NTP entry routes to the open promoter complex in the presence of DksA or TraR

(**A-D**) The iNTP (CPK representation) bound at the active site are viewed through the secondary channel (**A**: apo-form RNAP, **B**: RNAP–DksA/ppGpp, **C**: RNAP–DksA) and the main channel (**D**: RPo with DksA/ppGpp). Molecular surfaces of RNAP (white), DksA (red) and DNA (template DNA: dark green, non-template DNA: light green) are depicted, and the β'rim helix (yellow) and bridge helix (blue) of RNAP are highlighted.

(**E**) The main channel can be used for NTP entry of the RPo with DksA covering at the secondary channel. RNAP, DNA and DksA are depicted as surface, CPK and ribbon representations. β subunit is removed to see the main channel of RNAP. NTP molecules aligned along the NTP entry route from the main channel are shown in pink with CPK representation.

```
 -60                      -35                  -10        +1                +20
  |                                                       |                 |
5' CAGAAAATTATTTTAAATTTCCTCTTGTCAGGCCGGAATAACTCCCTATAATGCGCCACCACTGACACGGACTCTACGAG 3' rrnB P1
3' GTCTTTTAATAAAATTTAAAGGAGAACAGTCCGGCCTTATTGAGGGATATTACGCGGTGGTGACTGTGCCTGAGATGCTC 5'

5' ATTTAAAATTTATCAAAAAGAGTATTGACTTAAAGTCTAACCTATAGGATACTTACAGCCATCGAGAGGGACACGGGGAA 3' T7A1
3' TAAATTTTAAATAGTTTTTCTCATAACTGAATTTCAGATTGGATATCCTATGAATGTCGGTAGCTCTCCCTGTGCCCCTT 5'

5' GGATAAATATCTAACACCGTGCGTGTTGACTATTTTACCTCTGGCGGTGATAATGGTTGCATGTACTAAGGAGGTTGTAT 3' λP_R
3' CCTATTTATAGATTGTGGCACGCACAACTGATAAAATGGAGACCGCCACTATTACCAACGTACATGATTCCTCCAACATA 5'

5' GGATATAACGGCACAAGAAACGCTAGCTGGCCAGTCATCGACAACTTTATGGAAGGAGTAACACTATGGCTTATAAACAC 3' uspA
3' CCTATATTGCCGTGTTCTTTGCGATCGACCGGTCAGTAGCTGTTGAAATACCTTCCTCATTGTGATACCGAATATTTGTG 5'
```

Supplemental Figure 5. Promoter DNA sequences used for the measurement of the DksA binding to RNAP – promoter DNA complex (**Fig. 5**)

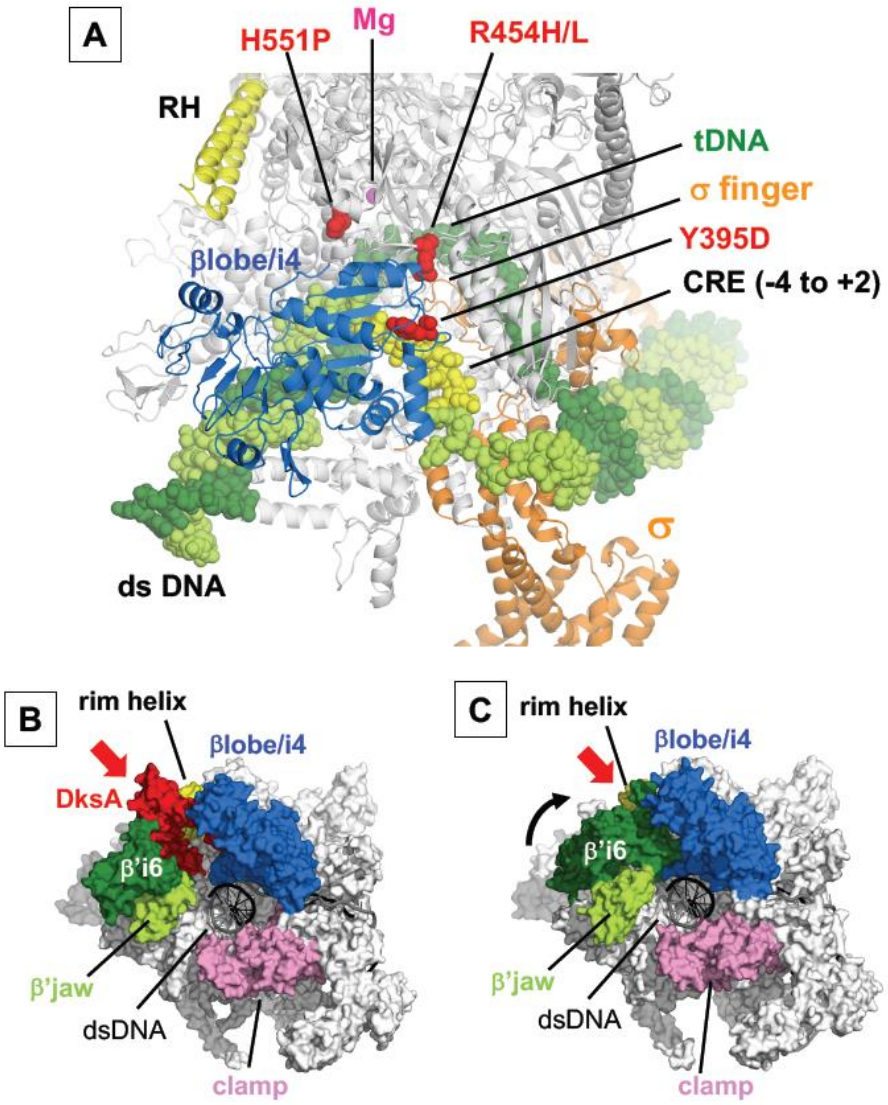

Supplemental Figure 6. The RNAP open promoter complex model.
(**A**) *E. coli* σ^{70} holoenzyme and open complex DNA model are depicted as ribbon and CPK representations, respectively. RNAP domains, σ subunit and core recognition element (CRE) of the non-template DNA are highlighted and labeled. *ΔdksA* suppressors (Rutherford et al., 2009) are shown as spheres and labeled. **(B-C)** *E. coli* σ^{70} RNAP holoenzyme and DksA are depicted as surfaces and DNA is depicted as a ribbon model. (**B**) the RPo model with DksA. (**C**) crystal structure of the initially transcribing complex (PDB: 4YLN). Pincers of the RNAP main channel (βlobe/i4 domain and β'clamp domain) and the downstream mobile element including β' jaw and β'i6 domains are highlighted and indicated. A gap between the βlobe/i4 and β'i6 used for the DksA accommodation is indicated by a red arrow in **B**, which is covered by the β'i6 after shifting its position. A movement of the β'i6 is indicated by a black arrow.

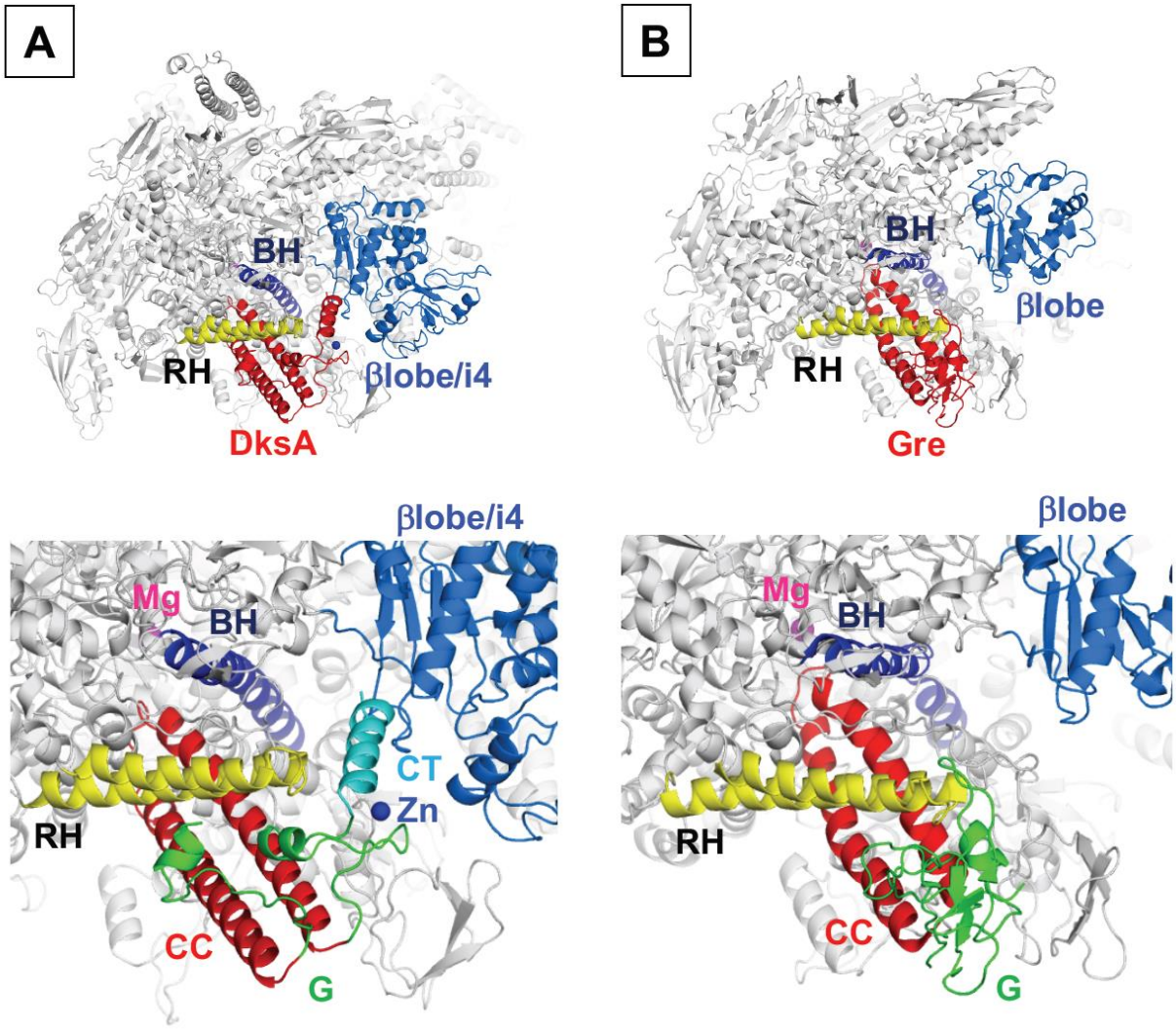

Supplemental Figure 7. Comparison between the DksA and Gre modes of binding to RNAP
Structures of the *E. coli* RNAP and DksA complex (**A**) and the *T. thermophilus* RNAP and Gre/Gfh1 chimera protein complex structures (**B**) (PDB: 4WQT). RNAP, DksA and Gre/Gfh1 are depicted as ribbon models. DksA and Gre/Gfh1 binding regions are magnified in the panels below and structural parts of DksA and Gre/Gfh1 chimera are indicated. The orientations of panels are the same as in a right panel of **Fig. 1A**.

Supplemental Movie 1. Assembly of DksA to RNAP triggers conformational changes in RNAP.

This movie shows RNAP conformational changes during the binary complex formation (from apo-form RNAP plus DksA to the binary complex). RNAP and DksA are depicted as ribbons, and domains and regions of RNAP and DksA are colored same as in Fig. 1A. The first scene shows a view from the RNAP main channel and the second scene shows a side view of RNAP, which contains the promoter DNA and the active site bound iNTP models.

Supplemental Movie 2. The conformational changes of DksA triggered by RNAP and ppGpp bindings.

This movie shows conformational changes in DksA triggered by the RNAP binding (first scene, from the apo-form to the RNAP bound binary complex) followed by ppGpp binding (second scene, from the binary to ternary complexes). Three structural parts of DksA and amino acid residues forming of the ΔppGpp suppressors (Super-DksA) are indicated.

Supplemental Movie 3. The ppGpp binding to the RNAP–DksA binary complex triggers conformational changes in RNAP and DksA.

This movie shows RNAP and DksA conformational changes during the ternary complex formation (from the binary complex plus ppGpp to the ternary complex). The first scene shows a view from the RNAP main channel and the second scene shows a side view of RNAP, which contains the promoter DNA and the active site bound iNTP models.